Journal of Hydrology 677 (2026) 135850

Contents lists available at ScienceDirect

Journal of Hydrology

journal homepage: www.elsevier.com/locate/jhydrol

Research papers

Offshore wind farms' impact on phytoplankton carbon and water quality: A multimethod analysis☆

Xinglong Guo [a], Guoqing Li [a,*], Hongyuan Shi [b,c], Lingrui Guo [d,e], Jing Yu [e]

[a] School of Resources and Environmental Engineering, Ludong University, Yantai 264025, China
[b] Institute of Coastal Research, Ludong University, Yantai 264025, China
[c] School of Hydraulic and Civil Engineering, Ludong University, Yantai 264025, China
[d] Key Laboratory of Physical Oceanography, Ocean University of China, Qingdao 266100, China
[e] College of Oceanic and Atmospheric Sciences, Ocean University of China, Qingdao 266100, China

ARTICLE INFO

Keywords:
Hydrodynamics
Eutrophication
Phytoplankton carbon concentration
Remote sensing

ABSTRACT

Offshore wind farms can affect marine ecosystems by altering phytoplankton carbon concentration and water quality. However, most existing studies rely on single observation methods, limiting a comprehensive understanding of these impacts. In this study, field measurements, remote sensing, and numerical simulations were integrated to assess the effects of offshore wind farms on surrounding phytoplankton carbon and water quality, and to explore their relationships. The results showed that (1) the integrated approach effectively captured both large-scale patterns and local dynamic changes in phytoplankton carbon concentration and water quality; (2) offshore wind farms increased phytoplankton carbon and chlorophyll-a concentrations. In summer, the phytoplankton carbon and chlorophyll-a concentrations inside the wind farm were more than twice those outside the wind farm; in winter, the phytoplankton carbon and chlorophyll-a concentrations inside the wind farm were approximately 1.5 and 1.1 times those outside, respectively; (3) dissolved oxygen, inorganic nitrogen, and inorganic phosphorus also increased inside the wind farm. Compared with those outside the wind farm, their increases were 2.93%, 45.72%, and 41.0% in summer, and 1.12%, 39.04%, and 49.59% in winter, respectively. (4) changes in phytoplankton carbon and chlorophyll-a were mainly driven by wind-farm-induced disturbances to the local flow field, rather than by nutrient limitation.

1. Introduction

Driven jointly by anthropogenic interventions and global climate change, significant changes are taking place in regional-scale water cycles, energy cycles, and carbon cycles across both terrestrial and marine systems. The spatiotemporal patterns of terrestrial water storage and extreme hydrological events are being continuously reshaped, increasing the uncertainty of regional water-resource management and ecological stability (Abhishek and Kinouchi, 2021; Abhishek et al., 2021; Xiong et al., 2022). Meanwhile, the imbalance in the Earth's energy budget and the continued accumulation of ocean heat have led to ocean warming, intensified marine heatwaves, cryosphere melting, and sea-level rise, further altering regional climate regulation and ecological environmental conditions (Venegas et al., 2023). With the continued accumulation of greenhouse gases, the carbon sink functions of both land and ocean tend to weaken under the combined effects of climate change and land-use disturbance. At the same time, as the ocean absorbs more atmospheric CO_2, ocean acidification and deoxygenation are intensified, adversely affecting the structure and function of marine ecosystems (Bijma et al., 2013). Against this background, carbon neutrality has become an important global strategic goal for addressing climate change and promoting green and low-carbon transformation. The world is accelerating its transition to renewable energy systems (De La Peña et al., 2022), and renewable energy is increasingly becoming a core component of national energy policies (Potrč et al., 2021).

The world is accelerating its transition to renewable energy systems with renewable energy gradually becoming a key component of national energy policies. Offshore wind power, as an important renewable energy source, is increasingly becoming a crucial part of the global energy transition due to its abundant offshore wind resources, lower wind

☆ This article is part of a special issue entitled: 'Water-Carbon processes' published in Journal of Hydrology.

* Corresponding author.
E-mail address: ligqing@foxmail.com (G. Li).

https://doi.org/10.1016/j.jhydrol.2026.135850

Available online 8 June 2026

shear, and higher energy production (Li et al., 2020). Moreover, compared to onshore wind farms, offshore wind farms can typically harness more stable and stronger wind, reduce competition for land resources, and avoid interference with human activities. Therefore, offshore wind farms have gradually become a focal point for energy development in many countries (Chen and Lin, 2022).

Despite the significant potential of offshore wind farms in carbon reduction and increasing renewable energy production, (Bailey et al., 2014) indicated that the construction and operation of offshore wind farms can have potential environmental impacts. (Nunneri et al., 2008) suggested that the construction of offshore wind farms leads to disturbance of seabed sediments, affecting the habitat of surrounding marine organisms. (Lindeboom et al., 2011) pointed out that offshore wind farms may alter water flow patterns, potentially impacting the distribution of marine plants. Additionally, research by (Bergström et al., 2014) found that the electromagnetic fields generated by offshore wind farms could interfere with the activities of surrounding marine organisms. Therefore, as offshore wind farms continue to expand in scale, the potential environmental issues associated with their development should not be overlooked.

To explore the potential impacts of offshore wind farms on phytoplankton carbon (PC) concentration and water quality, (Kordan and Yakan, 2024) used in-situ data, with chlorophyll-a (Chl-a) concentration as a representative indicator of phytoplankton biomass, to analyze the impact of offshore wind farms on phytoplankton populations in the North Sea. The results showed that the construction and operation of offshore wind farms reduced the richness of phytoplankton. (Wang, Ru, et al., 2023) collected numerous samples data from the Putaodao offshore wind farm in China, finding that the concentration of heavy metals in the water near the center of the wind farm increased. Similarly, (Hong et al., 2024) conducted field surveys to collect water quality data from the Guishan offshore wind farm and used indices such as the Shannon-Weaver index to describe the phytoplankton community structure. The results indicated that the operation of offshore wind farms had a minimal impact on the structure of the phytoplankton community.

Field survey sampling has provided valuable evidence for assessing the impact of offshore wind farms on PC concentration and water quality. However, the high cost of data collection and the limited spatial coverage restrict the feasibility of large-scale studies. To overcome these limitations, (Lecordier et al., 2025) attempted to use remote sensing to assess the impact of wind turbines in offshore wind farms on water quality. They found that offshore wind farms affect the concentration of suspended particulate matter around the wind turbines. (Lu et al., 2022) used remote sensing data to evaluate the impact of offshore wind farms on Chl-a concentration, finding a clear aggregation of Chl-a around the turbines. These studies provide important references for using remote sensing data to monitor the impact of offshore wind farms on water bodies. However, they also found that while remote sensing technology enables low-cost and large-scale monitoring of water quality changes, its temporal and spatial resolution limitations make it difficult to describe in detail the impacts of offshore wind farms on water bodies.

To address these issues, (Floeter et al., 2017) employed a combination of in-situ data and numerical simulations to more precisely assess the impact of offshore wind farms on water quality in three-dimensional space. Using an offshore wind farm in the North Sea of Europe as a case study, they evaluated the impact of offshore wind farms on phytoplankton and Chl-a concentrations. Their findings indicated that while the concentration of Chl-a increased, the phytoplankton biomass did not show a widespread increase. The advantage of numerical simulations lies in their ability to handle the complex interactions between hydrodynamics and ecological processes, simulating dynamic processes such as water flow, nutrient cycling, and community changes, and projecting the trends and patterns of water quality and ecosystem evolution (Ganju et al., 2015). However, numerical simulations require a large amount of in-situ data input, which limits their application on a large scale.

In this study, we aim to develop an approach that integrates the advantages of in-situ measurements, remote sensing, and numerical simulations to assess the impact of offshore wind farms on PC concentration and water quality. The significance of this research lies in the following: (1) combining the efficiency and broad coverage of remote sensing data with the detail and accuracy of numerical simulations, we propose a multi-scale research method to evaluate the potential impacts of offshore wind farms on PC concentration and water quality; (2) by coupling hydrodynamic and eutrophication models, we analyze the relationship between PC concentration and water quality in offshore wind farms, identifying key factors that influence PC.

2. Data

2.1. Study area

The study area of this research is the Dalian Zhuanghe Offshore Wind Farm, located off the eastern side of Shicheng Island in Zhuanghe City, Liaoning Province, China, as shown in Fig. 1. This offshore wind farm is the largest in northern China, situated approximately 35.2 kilometers from the shore, with a planned area of 55.8 square kilometers and a total installed capacity of 650 MW. The average water depth in the area is 30 meters.

2.2. In-situ data

2.2.1. Tide and current data

Tidal and current data were obtained through in-situ measurements at water level monitoring stations, as shown in Fig. 1 (b). We used the Signature1000 Acoustic Doppler Profiler to measure hydrodynamic parameters such as water levels, current velocity, and current direction. This device is known for its high precision and stability, capable of real-time recording of tidal variations and water flow characteristics, providing reliable data for subsequent hydrodynamic simulations.

The data were collected from May 16, 2023, to July 31, 2023, with a time interval of 10 minutes. These measurements offer a detailed understanding of the tidal and current dynamics in the area around the Dalian Zhuanghe Offshore Wind Farm, which is crucial for assessing the environmental impacts.

2.2.2. Depth data

The bathymetric data were obtained from the China Maritime Electronic Chart Service (https://www.chart.msa.gov.cn/customer/home), which fully covers the study area. The data points are spaced between 1 to 4 kilometers apart, allowing for effective capture of the variations in the seabed topography in the region.

These depth measurements provide a detailed and accurate representation of the seabed topography, which is crucial for understanding the hydrodynamic conditions, sediment dynamics, and ecological processes, such as nutrient distribution and phytoplankton growth, in the vicinity of the Dalian Zhuanghe Offshore Wind Farm. The data are also vital for improving the accuracy of hydrodynamic models used to assess the potential environmental impacts of the wind farm.

2.2.3. Water quality data

The water quality data were sourced from the Marine Water Quality Monitoring Information Public System (http://ep.nmemc.org.cn:8888/Water/). Key water quality indicators, including dissolved oxygen (DO), inorganic nitrogen (IN), and soluble reactive phosphorus (SRP), were selected for this study. SRP was chosen as an indicator of dissolved inorganic phosphorus (IP) due to its high proportion in the IP fraction of seawater (Liu, Mao, et al., 2024).

The data cover two periods: May and July 2023 (summer), and October and December 2023 (winter), with a total of 47 samples. The sampling sites for water quality data are shown in Fig. 1 (b). The measurements of DO, IN, and IP are crucial for understanding the nutrient dynamics and overall water quality in the study area, and for assessing

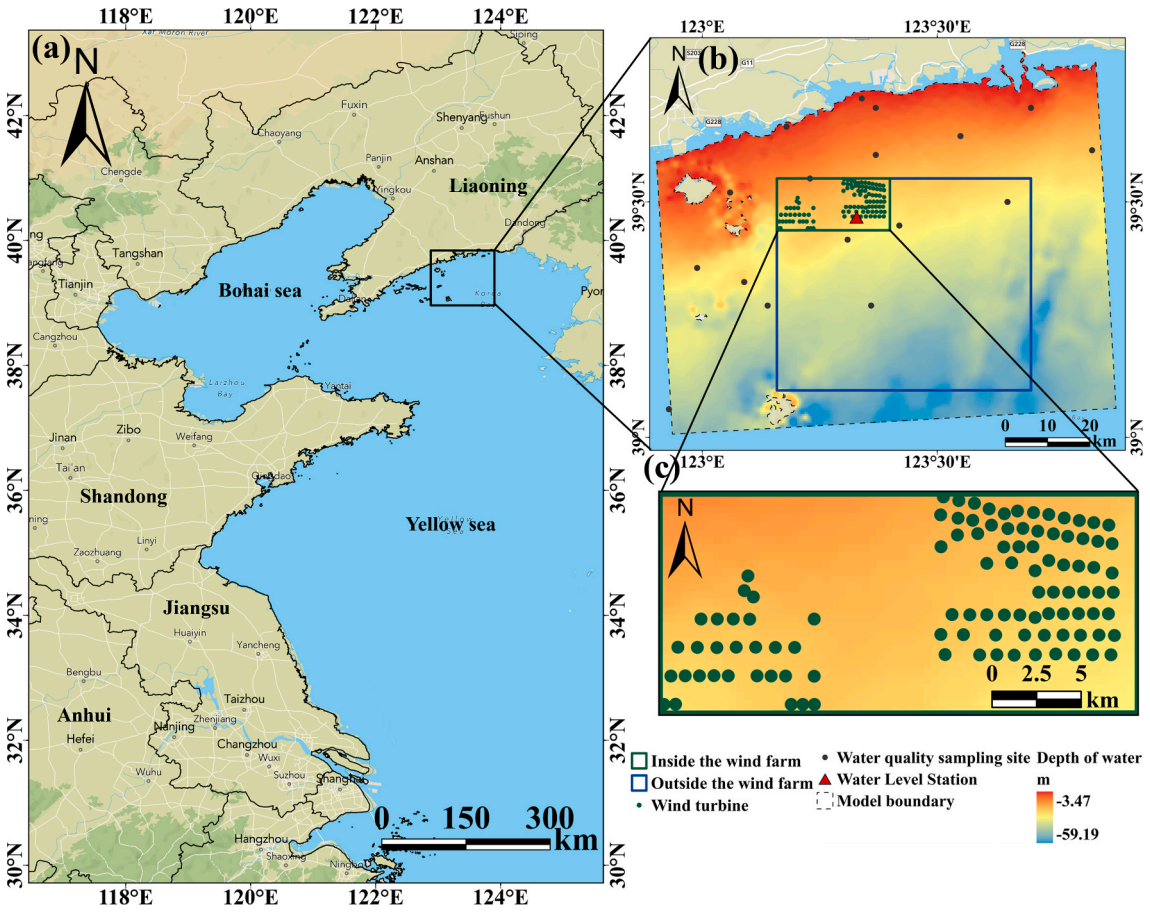

Fig. 1. Location of the study area (a) The geographic location of the Dalian Zhuanghe Offshore Wind Farm. (b) The coverage area of numerical simulations and remote sensing imagery. (c) Comparison areas inside and outside the wind farm.

the potential impact of the offshore wind farm on the surrounding marine environment.

2.3. Remote sensing data

2.3.1. Phytoplankton carbon concentration data

This study used the MODIS L2B GIOP (Global Ocean Observing Platform) data product (https://modis.gsfc.nasa.gov/data/dataprod/Cphyt.php). These data are processed from the raw observations obtained by the MODIS satellite through various steps, including algorithmic processing, atmospheric correction, and geographic correction. (Graff et al., 2015) applied this data for the calculation of PC concentration, and the results indicated that this method provides high accuracy and reliability. We selected data from two periods: May 1 to July 31, 2023 (summer), and October 1 to December 31, 2023 (winter). A total of 87 images covering the study area were screened, including 38 images in summer and 49 images in winter, with a spatial resolution of 1 km.

2.3.2. Chlorophyll-a concentration products

The Chl-a concentration product used in this study MODIS L2.OC product, which is derived from atmospheric correction, sea surface reflectance processing, and pigment concentration inversion algorithms. This product effectively eliminates the influences of atmospheric and sea surface reflections, providing accurate Chl-a concentration measurements (Bailey and Werdell, 2006). In situ measurement data were used as ground truth to validate the Chl-a concentration product, and (Hu et al., 2019) conducted a global evaluation of the product, which demonstrated that the MODIS Chl-a concentration product is highly reliable. We selected Chl-a concentration data from two periods: May 1 to July 31, 2023 (summer), and October 1 to December 31, 2023 (winter). A total of 87 Chl-a images covering the study area were screened, including 38 images in summer and 49 images in winter, with a spatial resolution of 1 km.

3. Methods

3.1. Numerical simulation

3.1.1. Hydrodynamic process simulation

We constructed a hydrodynamic model based on the fluid dynamics equations and boundary control conditions to simulate hydrodynamic processes. This model is widely used in hydrology, hydraulic engineering, marine environmental studies, and ecosystem simulations, as it effectively simulates water flow, tides, waves, wind fields, and their interactions with environmental factors (Jia et al., 2018). The model assumes the hydrostatic approximation and the Boussinesq approximation, with the governing fluid dynamics equations being describable in a Cartesian coordinate system (Zhang et al., 2023).

(1) Fluid dynamics equations

$$\frac{\partial u}{\partial x}+\frac{\partial v}{\partial y}+\frac{\partial w}{\partial z}=S \tag{1}$$

$$\frac{\partial u}{\partial t}+\frac{\partial u^2}{\partial x}+\frac{\partial vu}{\partial y}+\frac{\partial wu}{\partial z}=$$

$$fv - g\frac{\partial \eta}{\partial x} - \frac{1}{\rho_0}\frac{\partial P_a}{\partial x} - \frac{g}{\rho_0}\int_z^{\eta}\frac{\partial \rho}{\partial x}dz - \frac{1}{\rho_0 h}\left(\frac{\partial s_{xx}}{\partial x} + \frac{\partial s_{xy}}{\partial y}\right) + \frac{\partial}{\partial z}\left(v_t\frac{\partial u}{\partial z}\right) + F_u + u_s S \tag{2}$$

$$\frac{\partial v}{\partial t} + \frac{\partial v^2}{\partial y} + \frac{\partial vu}{\partial x} + \frac{\partial wv}{\partial z} = -fu - g\frac{\partial \eta}{\partial y} - \frac{1}{\rho_0}\frac{\partial P_a}{\partial y} - \frac{g}{\rho_0}\int_z^{\eta}\frac{\partial \rho}{\partial y}dz - \frac{1}{\rho_0 h}\left(\frac{\partial s_{yx}}{\partial x} + \frac{\partial s_{yy}}{\partial y}\right) + \frac{\partial}{\partial z}\left(v_t\frac{\partial v}{\partial z}\right) + F_v + v_s S \tag{3}$$

where x, y, and z are coordinates in the Cartesian coordinate system; η is the symbol indicating the elevation of the surface; d denotes the depth of the water at rest; h=η+d is the representation of the depth of the total water; u, v, and w are the velocity components in the x,y, and z directions; f is the Coriolis force parameter; g represents the gravitational acceleration; ρ is the density of seawater; s_{xx},s_{xy},s_{yx}, and s_{yy} represent the component of the radiation stress tensor in the x,y direction; v_t represents the vertical eddy viscosity coefficient; Pa is the representation of the pressure of the atmosphere; ρ_0 is the representation of the density of water at a reference state; S is the point source discharge amount; and u_s, v_s are the component velocities in the x and y directions when discharged into the water body.

(2) Boundary control conditions

Land Boundary (Eq. (4)):
Flow Velocity:

$$\vec{V} \times \vec{n} = 0 \tag{4}$$

Open Boundary Conditions (Equations (5)–(7)):
Water level:

$$\zeta(x,y,t)|_{\Gamma} = \zeta^{*}(x,y,t) \tag{5}$$

Velocity:

$$u(x,y,t)|_{\Gamma} = u^{*}(x,y,t) \tag{6}$$

$$v(x,y,t)|_{\Gamma} = v^{*}(x,y,t) \tag{7}$$

3.1.2. Phytoplankton carbon concentration and water quality

After constructing the hydrodynamic model, we used the eutrophication model to simulate PC concentration and water quality. This model is built on the foundation of the hydrodynamic model, allowing for tight coupling between the two. The model is capable of simulating the growth, reproduction, and mortality processes of phytoplankton and zooplankton, and it provides a detailed description of the nutrient cycling processes in the water body (Guo et al., 2025). The ecological processes in the eutrophication model are shown in Fig. 2 (Flindt and Kamp-Nielsen, 1997).

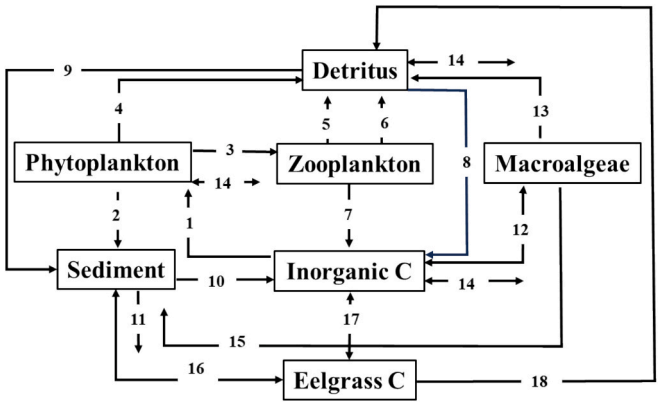

Fig. 2. Ecological processes of the eutrophication model.

The water quality model: (1) Phytoplankton production; (2) Phytoplankton sedimentation; (3) Grazing; (4) Phytoplankton death; (5) Zooplankton excretion; (6) Zooplankton death; (7) Zooplankton respiration; (8) Mineralization of suspended detritus; (9) Detritus sedimentation; (10) Sediments mineralization; (11) Sediment accumulation; (12) Macroalgae production; (13) Macrophyte sloughing; (14) External exchange; (l5) Sedimentation of macroalgae; (16) Eelgrass; (17) Eelgrass production; (18) Eelgrass sloughing.

3.1.3. Grid setup and model initialization

In this study, we used an irregular triangular grid to discretize the computational domain. The grid density gradually increases from the inner sea to the outer sea. The offshore wind farm in the study area employs monopile-type turbines (Floeter et al., 2017; Rezaei et al., 2023), and the areas surrounding the turbines were treated as no-flow areas in the model (Cazenave et al., 2016; Hendriks et al., 2025). Therefore, a no-flow boundary condition was applied in the wind farm region, treating it as a static area. To ensure computational accuracy, we implemented local grid refinement around the wind turbines (see Fig. 3).

Furthermore, the entire model was vertically divided into five layers along the water depth, resulting in a total of 72,062 grid cells. In addition, we adopted a uniform sigma-layer scheme, dividing the water column vertically into five equal-proportion layers. This grid configuration allows for precise modeling of hydrodynamic and ecological processes, ensuring that the model can accurately simulate the interactions between water movement, nutrient cycling, and the effects of the offshore wind farm on the surrounding marine ecosystem.

The simulation periods of the model were from 00:00 on May 1, 2023 to 00:00 on July 31, 2023 (summer), and from 00:00 on October 1, 2023 to 00:00 on December 31, 2023 (winter), with a time step of 1 hour. During these period, the model was validated using measurement data. The influence of the initial water level on the simulation results was found to be minimal, and the model reached a stable state after running for a period of time. Therefore, we adopted a cold start approach, assuming that the initial flow velocity and water level across the entire domain were both zero.

For the eutrophication model, the initial values were taken from the average concentrations of PC, Chl-a, DO, IN, and IP data collected in May. This approach allowed for a more accurate representation of the initial conditions in the study area, ensuring that the model could simulate the nutrient and ecological dynamics effectively.

3.2. Calculations using remote sensing data

The PC concentration was derived from the MODIS L2B GIOP data product, specifically bbp_s_giop and bbp_443_giop. The backscattering coefficient at a wavelength of 470 nm, denoted as bbp_470, is calculated based on the relationship between bbp_443_giop and the slope coefficient bbp_s_giop. The formula is as follows (Graff et al., 2015):

$$bbp\_470 = bbp\_443\_giop\left(\frac{470}{443}\right)^{bbp\_s\_giop} \tag{8}$$

where bbp_443 represents the backscattering coefficient at a wavelength of 443 nm, and bbp_s_giop is the slope coefficient, which characterizes the spectral shape and is dimensionless.

The relationship between PC concentration (carbon_phyto) and bbp_470 is described by the following linear equation:

$$carbon\_phyto = a1(bbp\_470) + b1 \tag{9}$$

where a1 = 12128 and b1 = 0.59, dimensionless. According to this formula, the backscattering coefficient bbp_470 is calculated using Equation (8), and the PC concentration is subsequently obtained, with

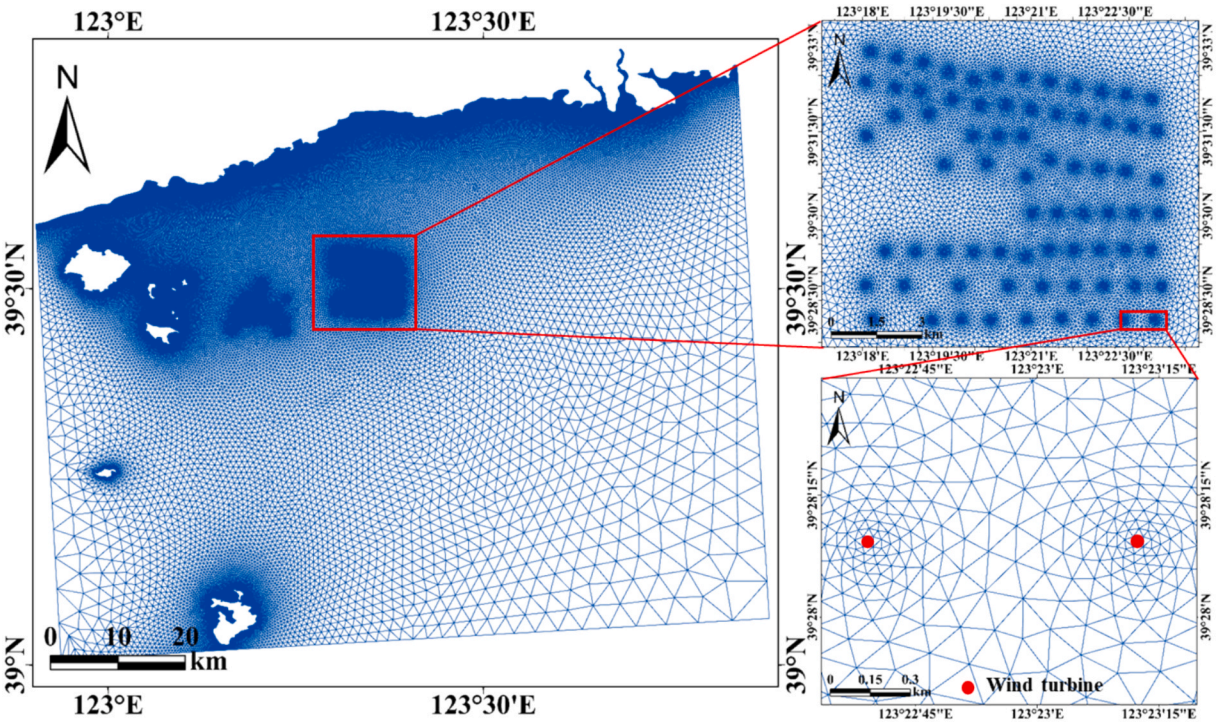

Fig. 3. Model grid.

units in mg/L.

4. Results

4.1. Simulation results validation

4.1.1. Validating tidal current speed and direction

To validate the accuracy of the hydrodynamic simulation results, we used tide, tidal current speed, and flow direction measured by the tide water level monitoring stations, as shown in Fig. 1. The Pearson correlation coefficient (PCC) was selected to measure the linear correlation between the simulated results and the observed data. A PCC value of 1 indicates no difference between the simulated and observed values. When the PCC exceeds 0.65, the simulation results are considered excellent. Values between 0.65 and 0.5 are considered very good, while values between 0.5 and 0.2 are rated as good. When the PCC is less than 0.2, the results are regarded as poor. A value of 0 indicates complete disagreement between the simulation and measured values (Zhang et al., 2023).

The validation period covered 77 data records, corresponding to 00:00 GMT each day from May 16, 2023 to July 31, 2023. Considering that the model requires an initial adjustment period under the cold-start condition, we used the data after the model had run for half a month and reached a relatively stable state for validation. As shown in Fig. 4, both the variations in water level and the high and low tide values are nearly identical between the calculated and measured values, with the timing of high and low tide events also being in close agreement. The calculated PCC was 0.99, indicating a strong correlation between the simulated and measured water levels, and the simulation results exhibit minimal deviation from the actual conditions.

We used the measured current velocity data at the water level monitoring stations to validate the model. The observed water depth at the station was 23.22 m. Each vertical layer corresponded to 20% of the local total water depth, with a thickness of approximately 4.64 m for each layer. After the model reached a stable state, we extracted the simulated current velocity and direction for each vertical layer at 00:00 each day from May 16, 2023 to July 31, 2023, and compared them with the observed data at the corresponding layers.

Fig. 5 (a)– (e) present the validation results of current velocity for each vertical layer at the water level monitoring stations. The results show that the model can reasonably reproduce the variation characteristics of current velocity at different vertical layers at this station. For the upper four layers, the overall variation trends of the simulated values are consistent with those of the observed values, with PCC values of

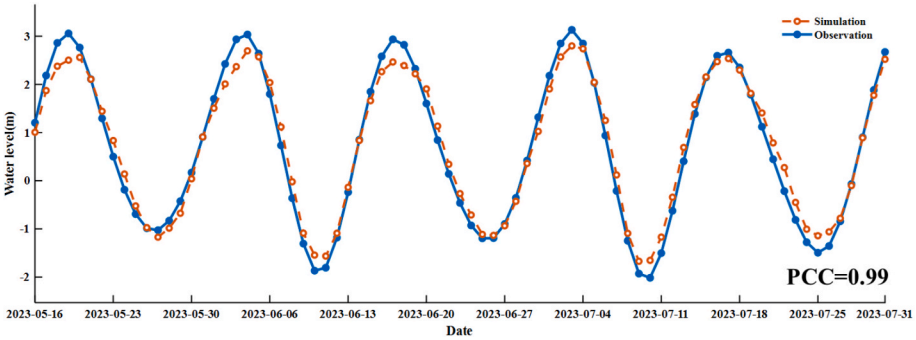

Fig. 4. Water level validation plot.

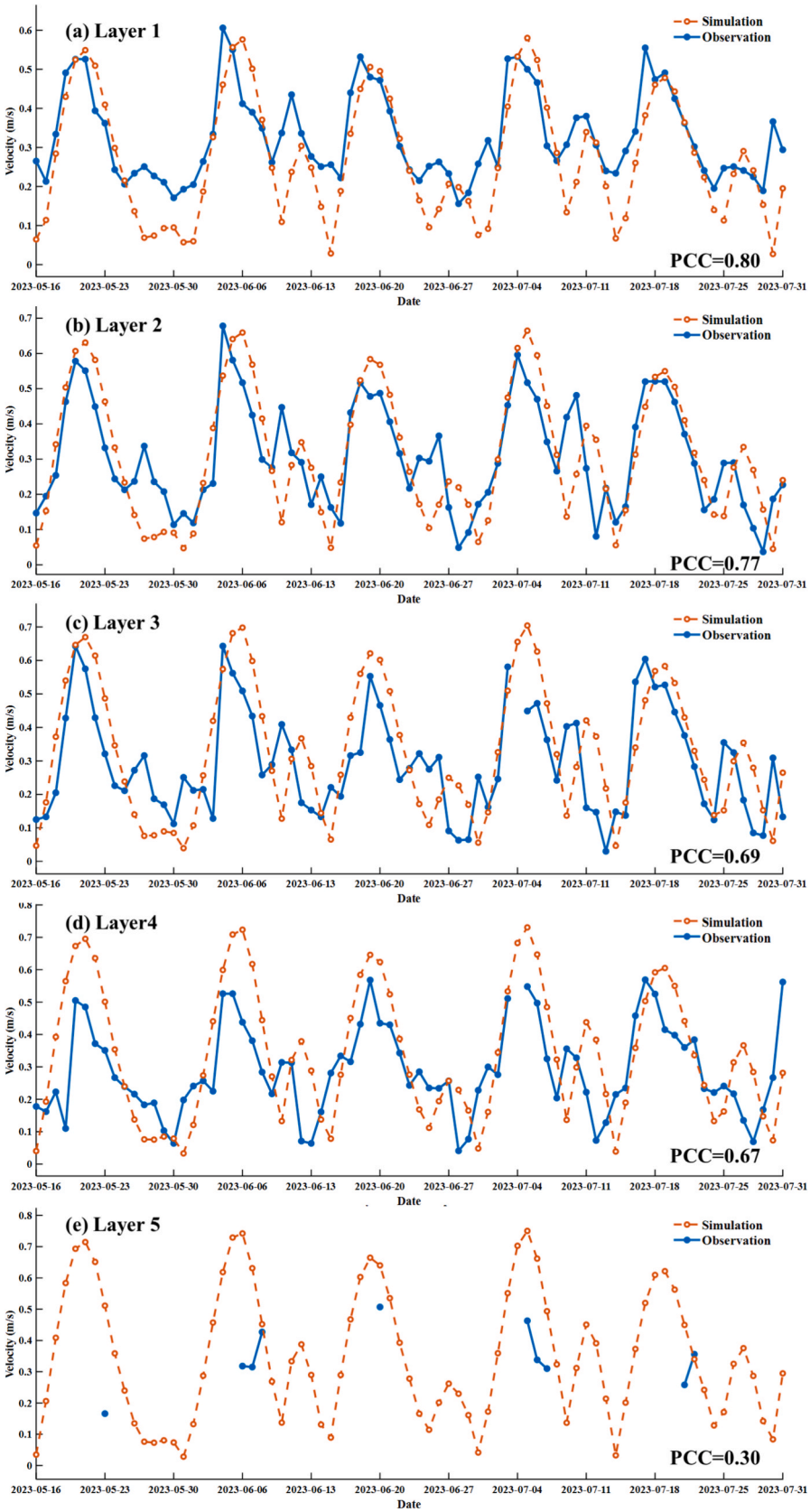

Fig. 5. Validation of tidal velocity.

0.80, 0.77, 0.69, and 0.67, respectively, indicating that the model has relatively high reliability in simulating current velocity from the surface to the middle layers. The PCC value for the fifth layer was 0.30, which was relatively low, mainly due to the large amount of missing near-bottom observational data and the limited sample size. Nevertheless, from an overall perspective, the model can still reasonably characterize the vertical structure of current velocity at this station, providing reliable hydrodynamic support for subsequent studies of water quality and ecological processes.

Fig. 6 (a)– (e) show the validation results of current direction for each vertical layer at the water level monitoring stations. For the upper four layers, the overall trends of the simulated results are generally consistent with those of the observed values, with PCC values of 0.53, 0.85, 0.55, and 0.31, respectively, indicating a reasonable consistency in the simulation of current direction changes from the surface to the middle layers, with the best performance found in Layer 2. In contrast, the PCC value for the fifth layer reached 0.90, indicating high consistency. However, because of the large amount of missing observed data and the limited sample size in this layer, the statistical result may have been affected by data completeness. Overall, the model can reasonably reflect the variation characteristics of current direction in the vertical profile at this station, thereby providing a reliable hydrodynamic basis for subsequent simulations of water quality and ecological processes.

4.1.2. Cross-validation: phytoplankton carbon and chlorophyll-a

We compared the eutrophication model results with remotely sensed PC and Chl-a data for validation. It should be noted that these two types of data differ substantially in their spatiotemporal characteristics and spatial representation, making direct comparison difficult. On the one hand, remote-sensing retrieval mainly relies on the optical signals from the ocean surface, therefore the obtained PC and Chl-a concentrations usually represent only the instantaneous surface values at the imaging time and cannot reflect the vertical distribution characteristics of the water body. On the other hand, remote-sensing data are continuous raster data with a spatial resolution of 1 km, whereas the model outputs are discrete spatial point data, and thus the two datasets are not consistent in either spatial resolution or data structure. To ensure comparability at the same spatial scale, we applied the Kriging interpolation method to reconstruct the model outputs into raster surfaces with the same spatial extent and resolution (1 km) as the remote-sensing data. Based on this, the monthly mean surface-layer (Layer 1) concentrations of PC and Chl-a during the summer and winter periods in the study area were extracted and compared with the remote-sensing retrieval results. Similarly, considering the initial adjustment process under the cold-start condition, we used the data after the model had run for half a month and reached a relatively stable state for validation. The cross-validation results for PC and Chl-a concentrations are shown in Fig. 7(a) and (b), respectively.

The height of the histogram represents the monthly average level of PC concentration, while the error bars indicate the fluctuation range between the maximum and minimum values for that month, providing a clearer visualization of the data variations.

Fig. 7 (a) compares the cross-validation results between the remotely sensed and simulated PC concentrations. Compared with the monthly mean values derived from remote sensing, the monthly mean simulated PC concentrations vary more smoothly, with relatively smaller fluctuations. In terms of seasonal comparison, the remotely sensed PC concentrations in summer are generally higher than the simulated results, with more obvious differences in May and June. In winter, however, the remotely sensed values decrease significantly, while the simulated results are relatively higher than the remote-sensing values. Overall, PC concentration shows a clear seasonal pattern, being higher in summer and lower in winter. The larger fluctuations in the remote-sensing results may be related to sensor observation conditions, sea-surface state, and the optical complexity of coastal waters.

The cross-validation results for Chl-a concentration are shown in Fig. 7 (b), and the overall pattern is generally consistent with that of PC. The model-simulated results change relatively smoothly, whereas the remotely sensed results show more obvious fluctuations. In summer, the remotely sensed Chl-a concentrations are generally higher than the simulated results, with a relatively large error range, indicating strong spatial heterogeneity and intra-month variability during this period. In winter, both the simulated and remotely sensed values decrease significantly, and the difference between them becomes smaller than in summer. Compared with PC, Chl-a still exhibits relatively large fluctuations in the remote-sensing results during winter, suggesting that it may be more sensitive to short-term environmental changes and the optical conditions of coastal waters.

Overall, the comparison results of PC and Chl-a indicate that the model simulations and the remote-sensing retrievals show good consistency in terms of seasonal variation, with both being higher in summer and lower in winter. Although some differences remain in the monthly mean concentration levels and fluctuation ranges, the model can reasonably reflect the seasonal variation characteristics of phytoplankton-related indicators in the study area. These differences may be associated with spatial errors introduced by Kriging interpolation and uncertainties inherent in remote-sensing retrievals, including sensor performance, interference from clouds and aerosols, sea-surface fluctuations, and the optical complexity of coastal waters.

4.1.3. Water quality data validation

We used the eutrophication model to calculate the monthly average concentrations of DO, IN, and IP in the study area, and compared these values with the monthly averages of the measured data. The measured water-quality data were mainly obtained from discrete sampling sites around the study area, and the sampling time scale was monthly. We also applied the Kriging interpolation method to spatially reconstruct the model outputs and generate raster surfaces with a spatial resolution of 1 km. Based on this, the monthly mean concentrations of DO, IN, and IP in the surface layer (Layer 1) during the summer and winter periods in the study area were calculated and compared with the monthly mean values of the measured water-quality data. The validation results for DO, IN, and IP concentrations are shown in Fig. 8.

As shown in Fig. 8 (a), the simulated DO concentrations are generally close to the observed values in both summer and winter, with both remaining within the range of approximately 7–9 mg/L. In comparison, the observed DO data show a larger error range, indicating certain intra-month or spatial fluctuations, and the resulting differences may be related to the spatiotemporal variability of the sampling sites. Overall, the model can reasonably reflect the monthly mean level of DO concentration in the study area.

As shown in Fig. 8 (b), the simulated IN concentrations are generally close to the observed values in May, July, and October, whereas the observed value in November is clearly higher than the simulated result. In terms of variation trends, the simulated results are relatively smooth overall, while the observed IN concentrations show much larger fluctuations and noticeably wider error bars, indicating strong uncertainty in the spatial distribution and intra-month variation of the observed IN concentrations. The model can reasonably reflect the overall level of IN concentration, but some deviations remain in representing high-value fluctuations in certain months.

As shown in Fig. 8 (c), the simulated IP concentrations are slightly higher than the observed values in summer, whereas in winter, the observed values are higher than the simulated results, with a relatively obvious difference in November. Similar to IN, IP also shows relatively large fluctuations. These large fluctuations are mainly due to the strong spatial heterogeneity and intra-month variability of the observed IP concentrations in the study area. In contrast, the simulated results vary more smoothly, indicating that the model can reflect the general magnitude of IP concentration, although its ability to capture local fluctuations in the observed data is relatively limited.

Overall, the comparison results of DO, IN, and IP indicate that the

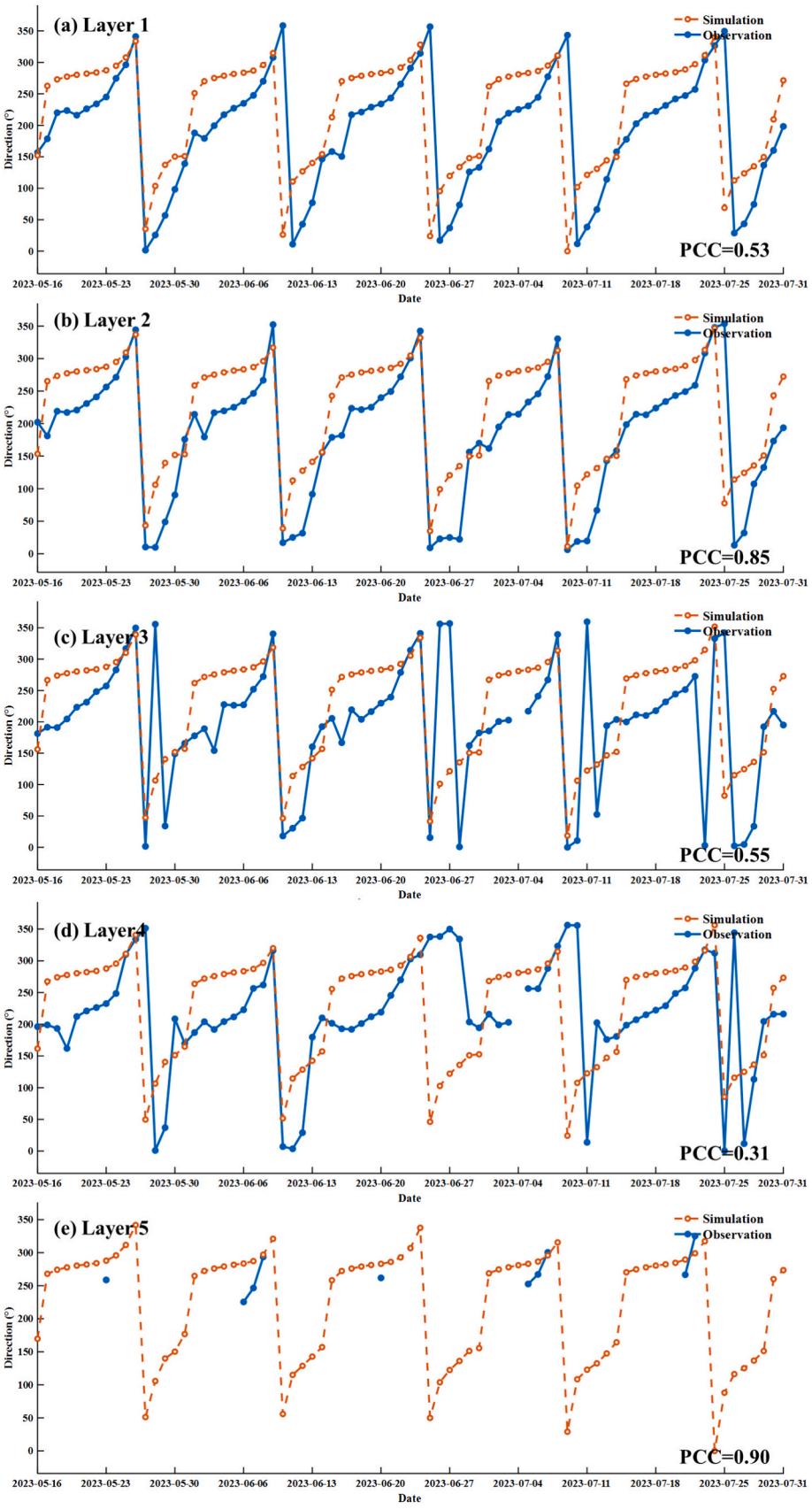

Fig. 6. Validation of tidal direction.

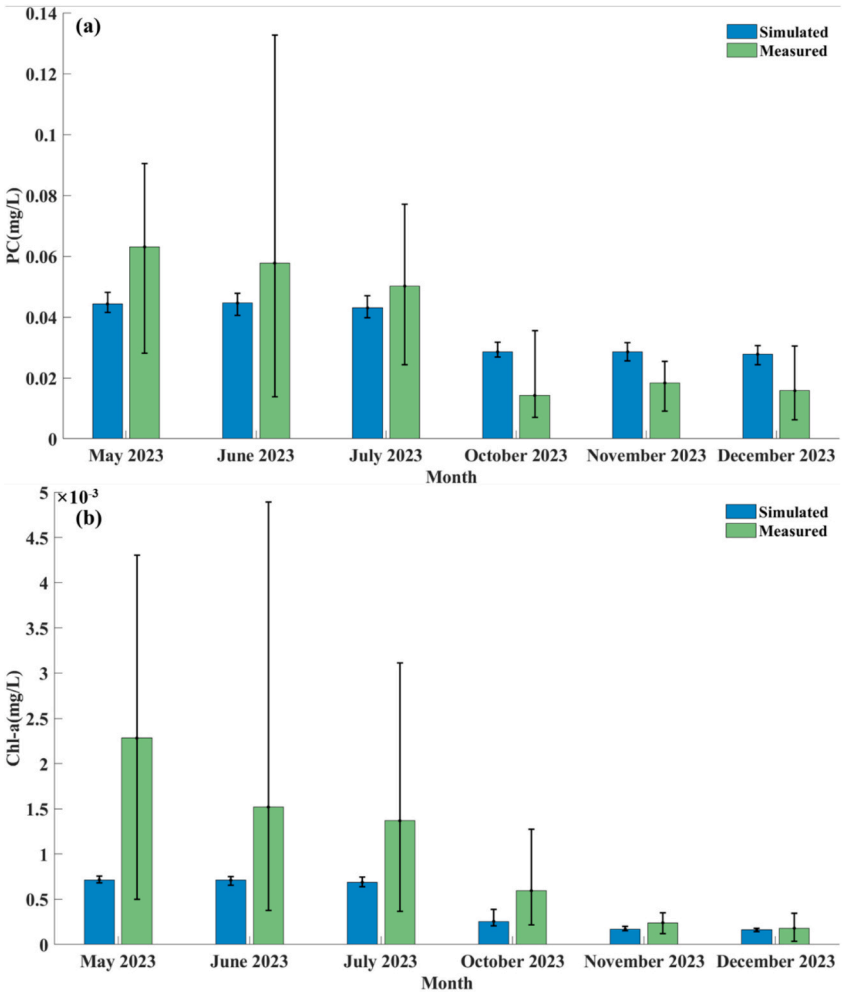

Fig. 7. Comparison of phytoplankton carbon and chlorophyll-a simulated values with remote sensing data.

eutrophication model simulations show a certain degree of consistency with the measured water-quality data in terms of monthly mean concentration levels. Among them, the DO simulation agrees relatively well with the observations, whereas IN and IP still show some deviations in certain months. These differences may be related to the limited number of sampling sites, their discrete spatial distribution, low sampling frequency, and spatial errors introduced during the Kriging interpolation process. In general, the model can reasonably reflect the monthly variation characteristics of the major water-quality indicators in the study area.

4.2. Variation of phytoplankton carbon concentration

4.2.1. MODIS remote sensing data

Based on the remote-sensing retrieval results, we analyzed the spatiotemporal variation characteristics of PC concentrations inside and outside the offshore wind farm. As shown in Fig. 9 (a)– (f), the PC concentrations in the study area exhibits clear spatial differences at the monthly scale. Overall, high-value areas of PC are mainly distributed within the wind farm and its adjacent waters. In most months, the PC concentrations inside or near the wind farm are higher than those in the surrounding offshore waters, indicating that a certain degree of PC accumulation may occur in the waters around the wind farm.

In terms of seasonal variation, PC concentrations are generally at a relatively high level in summer, especially in the vicinity of the wind farm and in the northwestern part of the study area, where obvious high-value areas are formed. In contrast, PC concentrations decrease overall in winter, and the extent of the high-value areas is significantly reduced; however, relatively high concentrations are still maintained within the wind farm and its adjacent waters. This indicates that PC concentrations in the study area exhibit clear seasonal variation, with generally higher values in summer and lower values in winter.

To quantitatively compare the differences in PC concentrations inside and outside the wind farm, the time series of PC concentrations in the inner and outer regions of the wind farm were extracted separately, as shown in Fig. 9 (g). Although PC concentrations both inside and outside the wind farm fluctuate to some extent, the PC concentration inside the wind farm is higher than that in the surrounding waters for most of the study period. From May to July, the PC concentration inside the wind farm remains at a relatively high level, and the difference from the outer region is relatively obvious. From October to December, the overall PC concentration decreases, and the difference between the inside and outside of the wind farm becomes smaller, but the concentration inside the wind farm still remains relatively higher overall.

This suggests that phytoplankton may accumulate in the waters surrounding the wind farm. We plotted the PC concentrations inside and outside the wind farm over time, as shown in Fig. 9g.

From Fig. 9 (g), although there is significant fluctuation in the PC concentrations inside and outside the wind farm, the concentration inside the wind farm remains consistently higher than in the surrounding areas. Oceanic factors such as tidal movements and currents may contribute to these fluctuations, but PC concentrations inside the wind farm consistently remains at higher levels, further supporting the idea of phytoplankton accumulation in the waters around the wind farm.

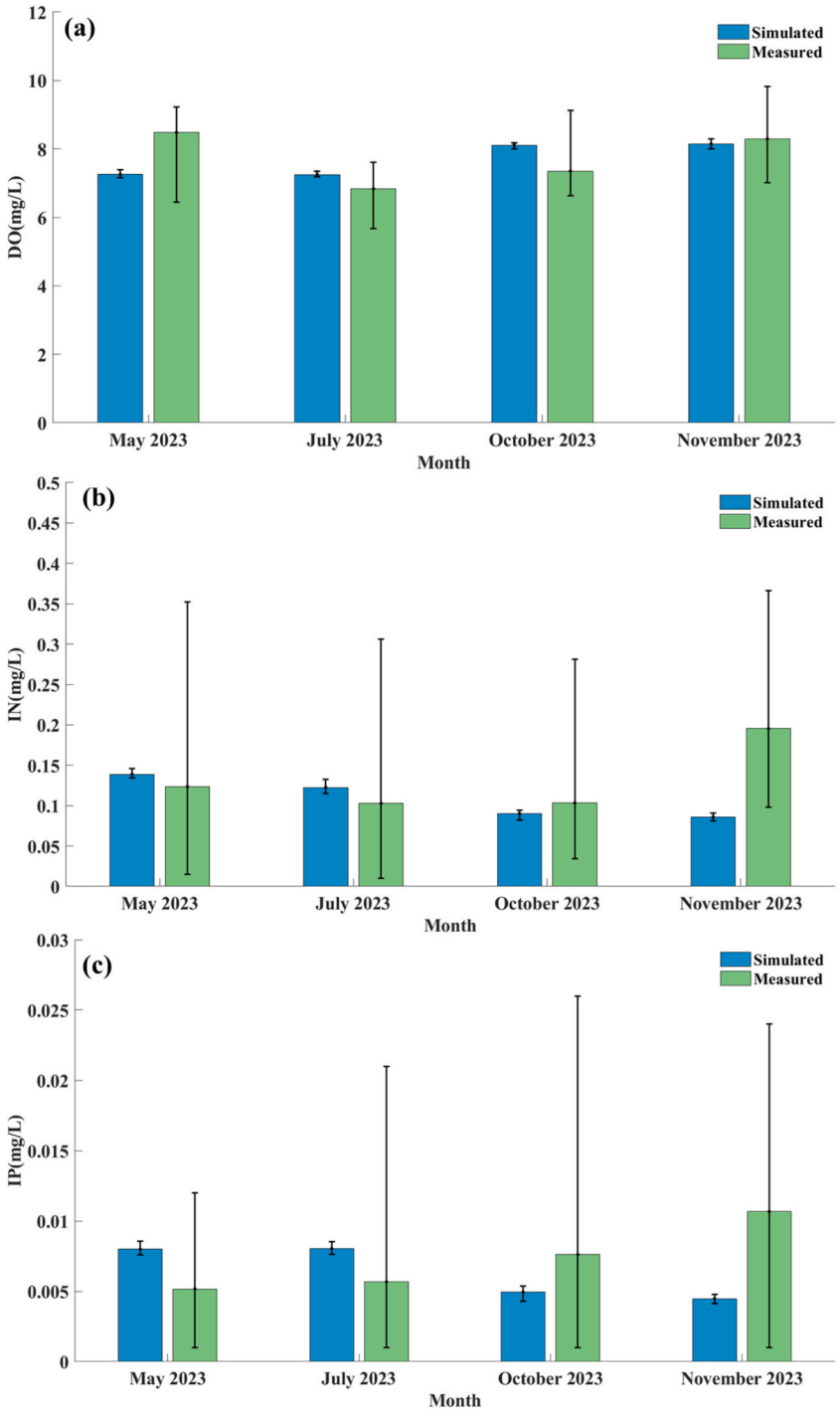

Fig. 8. Comparison between water quality simulation values and observational data.

Overall, the spatial distribution and time-series results in Fig. 9 jointly indicate that PC concentrations within the wind farm and its adjacent waters are generally higher than those in the outer region, suggesting that local PC accumulation may occur around the wind farm. Although PC concentrations shows some temporal fluctuations, which may be related to hydrodynamic processes such as tides and currents as well as seasonal environmental changes, the feature that PC concentrations inside the wind farm remain consistently higher than those in the outer region is relatively stable. This suggests that the wind-farm structures may have a certain influence on the spatial distribution of phytoplankton in the surrounding waters.

4.2.2. *Results of numerical simulation*

We analyzed the eutrophication model results after the model had reached a sufficiently stable state and selected the monthly mean PC concentrations for June, July, November, and December 2023 after applying Kriging interpolation. The horizontal distribution of the simulated eutrophication model results inside and outside the wind farm in June 2023 is shown in Fig. 10 (a), and the results for July are shown in Fig. 10 (b). The horizontal distributions for November and December are shown in Fig. 10 (d) and 10 (e), respectively. The three-dimensional distribution of PC concentration inside and outside the wind farm is shown in Fig. 10 (c), and the temporal variation of PC concentration is shown in Fig. 10 (f). As shown in Fig. 10 (a), the PC concentration inside

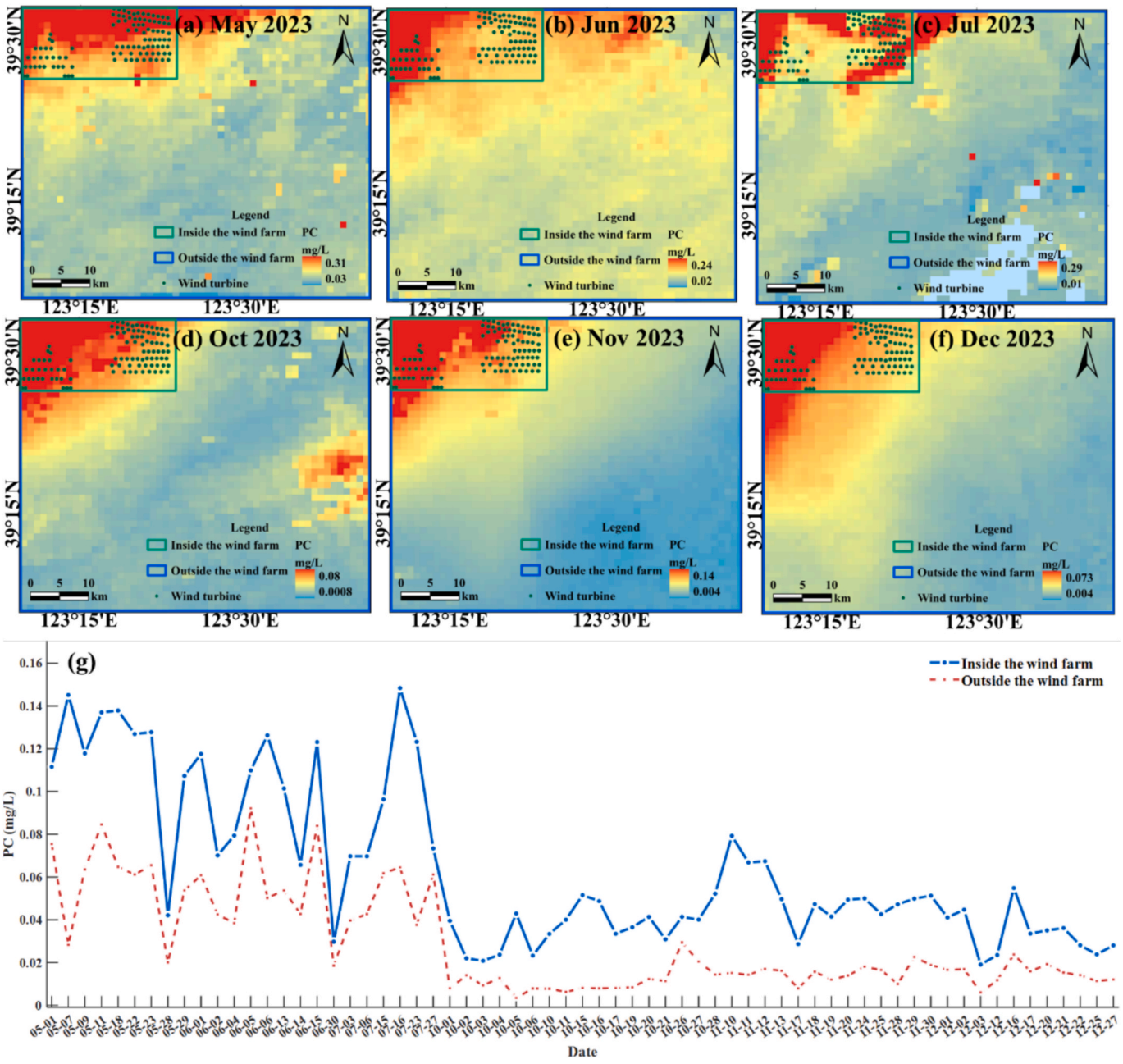

Fig. 9. Changes in phytoplankton carbon concentration inside and outside the wind farm based on MODIS data.

the wind farm is significantly higher than that outside, which is consistent with the observation from remote-sensing imagery. Fig. 10 (b) likewise shows that the concentration inside the wind farm is higher than that outside. In Fig. 10 (d) and 10 (e), during winter (November and December), the wind farm and its adjacent waters still maintain relatively high PC concentrations; however, the overall concentration is lower than that in summer, and the extent of the high-value areas is reduced.

From the two-dimensional analysis of both remote sensing and eutrophication model simulation results, that the PC concentration inside the wind farm is significantly higher than in the external regions. Both the remote-sensing observations and the simulation results indicate a clear aggregation of PC concentration near the wind farm. Additionally, the simulation further reveals the distribution characteristics of this aggregation effect over a larger spatial scale.

When examining the variation of PC concentration from a three-dimensional perspective, as seen in Fig. 10 (f), we observe that the concentration decreases with increasing water depth. In terms of seasonal variation, PC concentrations were generally higher in summer than in winter. In summer, the extent of the high-value PC areas was larger, and concentrations were higher in the vicinity of the wind farm. After entering winter, the overall PC concentration decreased, and the extent of the high-value areas was reduced; however, relatively high concentrations were still maintained within the wind farm and its adjacent waters, indicating clear seasonal variation in PC concentration in the study area. This pattern is generally consistent with the previously described remote-sensing results and model-validation results, both of which showed higher values in summer and lower values in winter.

The three-dimensional distribution results are shown in Fig. 10 (c). The difference in PC concentration between the inside and outside of the wind farm is not only reflected in the surface layer, but also exhibits obvious stratification in the vertical direction, with significant

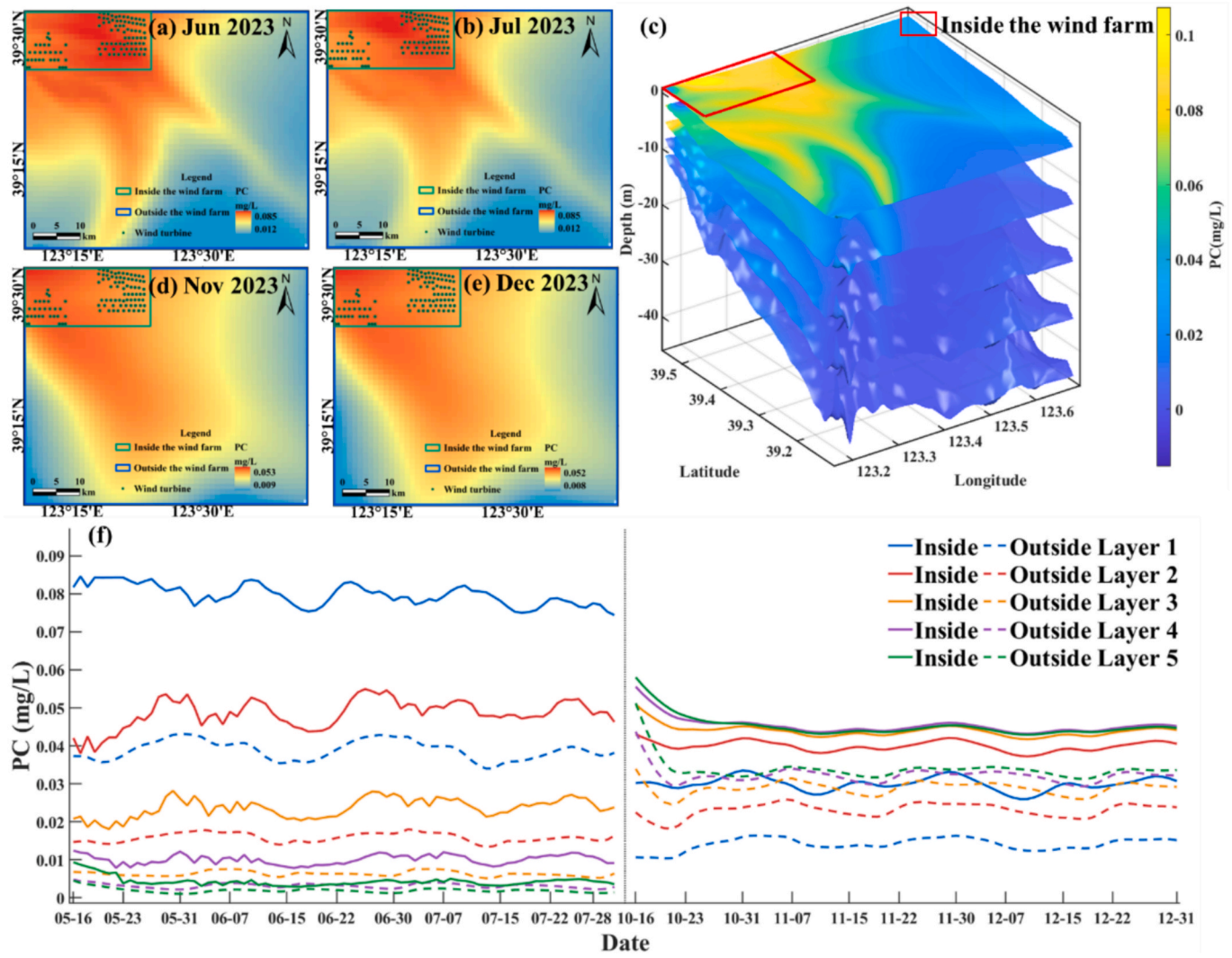

Fig. 10. Comparison of phytoplankton carbon concentration inside and outside the wind farm.

concentration differences among different water layers. Fig. 10 (f) further shows the temporal variation of PC concentrations inside and outside the wind farm at different vertical layers. In summer, PC concentrations both inside and outside the wind farm show clear vertical stratification, generally decreasing with increasing water depth. At the same time, PC concentrations in all layers inside the wind farm are generally higher than those outside, with the most obvious difference occurring in the surface layer, indicating a more significant accumulation of PC inside the wind farm during summer. It is worth noting that, in winter, the vertical distribution pattern of PC concentration changes to some extent. During some periods, the surface concentration is lower than the bottom concentration, showing a vertical distribution pattern different from that in summer. Meanwhile, the overall PC concentration in winter is significantly lower than that in summer, further demonstrating the clear seasonal variability of PC concentration in the study area.

The results in Fig. 10 indicate that the PC concentrations simulated by the eutrophication model exhibit obvious spatial differences in both the horizontal and vertical directions. Horizontally, PC concentrations within the wind farm and its adjacent waters are generally higher than those in the outer region, which is broadly consistent with the spatial distribution characteristics revealed by the remote-sensing observations. Vertically, PC concentrations are mainly concentrated in the upper water layers in summer and gradually decrease with increasing depth, whereas the vertical distribution pattern changes somewhat in winter. The difference in PC concentration between the inside and outside of the wind farm is more pronounced in summer and weakens in winter, but the inside of the wind farm still generally maintains relatively higher PC concentrations. These results suggest that a certain degree of PC accumulation may occur in the waters surrounding the wind farm and that this accumulation shows clear seasonal and vertical differences.

4.3. *Changes in water quality*

4.3.1. *Changes in chlorophyll-a concentration*

(1) Chlorophyll-a concentration shifts via remote sensing

Fig. 11 (a)– (f) show the monthly mean Chl-a concentrations for May, June, July, October, November, and December 2023, respectively. As shown in the figure, in May, June, July, November, and December, it can be observed that the concentration within the wind farm is higher than that outside the wind farm, although there are some pixels farther from the wind farm with relatively higher concentrations. In terms of seasonal variation, Chl-a concentrations were generally at a relatively high level in summer, especially in the vicinity of the wind farm and in the northwestern part of the study area, where obvious high-value areas were formed. In contrast, Chl-a concentrations decreased overall in winter, and the extent of the high-value areas was significantly reduced, with the concentration distribution in the study area becoming more uniform. This indicates that Chl-a concentration also shows clear seasonal variability, with generally higher values in summer and lower

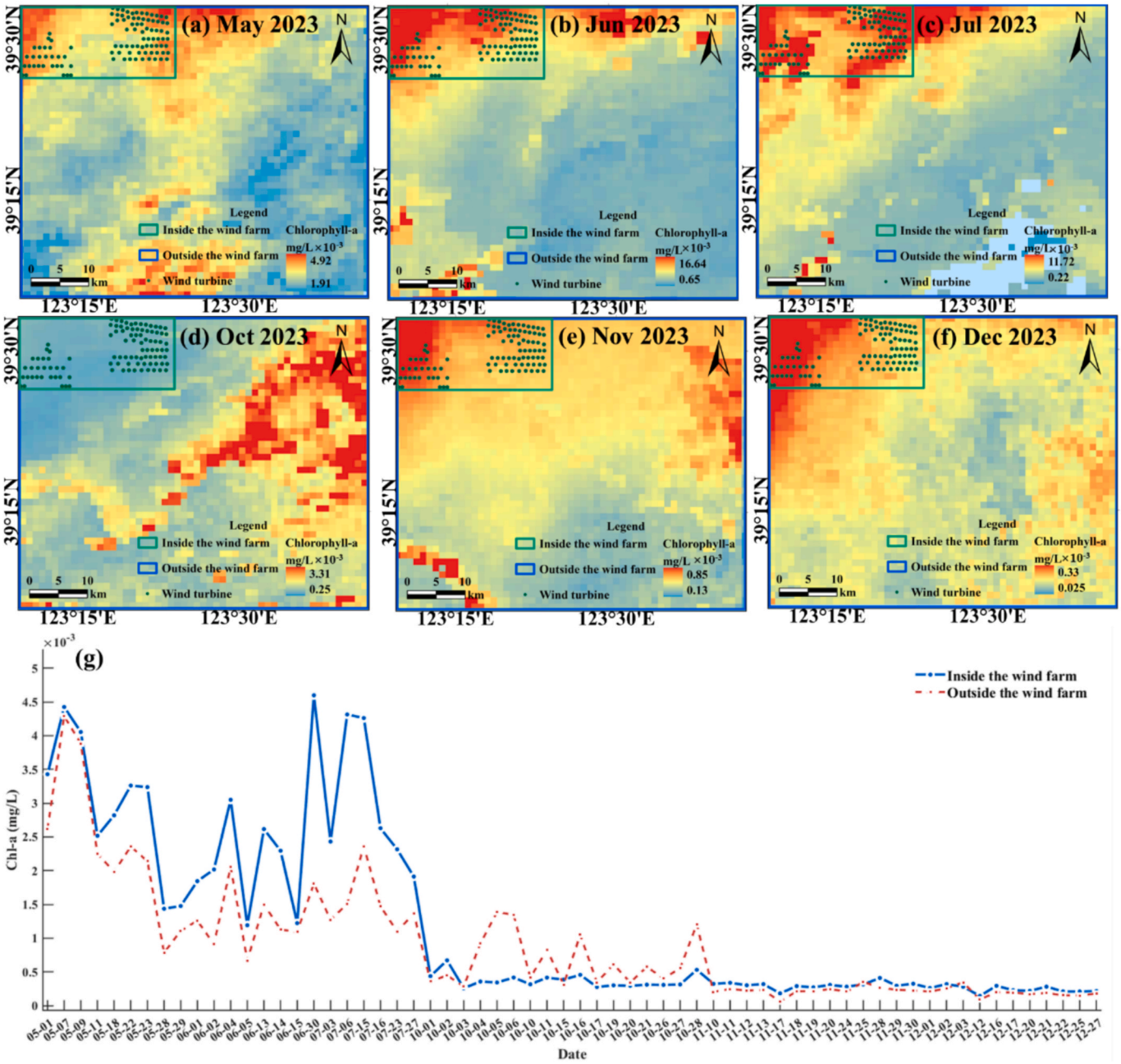

Fig. 11. Remote sensing observation of chlorophyll-a concentration differences inside the wind farm.

values in winter, a seasonal pattern that is broadly similar to that of PC. To further analyze this, we plotted a time series of Chl-a concentration both inside and outside the wind farm, as shown in Fig. 11 (g). As shown in the figure, during the period from May to July, Chl-a concentrations both inside and outside the wind farm exhibited obvious fluctuations; however, the Chl-a concentration inside the wind farm remained higher than that in the surrounding waters for most of the time, and the difference between the two was relatively clear. After October, the overall Chl-a concentration decreased significantly, and the difference between the inside and outside of the wind farm became smaller. During some periods, the concentrations in the two regions were relatively close, but the concentration inside the wind farm still remained relatively higher overall.

(2) Chlorophyll-a concentration shifts via numerical simulations

We selected the results of the eutrophication model after it reached full stability for our study. Fig. 12 (a), 11 (b), 11 (d), and 11 (e) present the monthly mean Chl-a concentrations for June, July, November, and December 2023, respectively, after applying Kriging interpolation to the results. The three-dimensional distribution of Chl-a concentration inside and outside the wind farm is shown in Fig. 11 (c), and the time variation of Chl-a concentration at different depths is shown in Fig. 12 (f).

In terms of seasonal variation, Chl-a concentrations were generally higher in summer than in winter. In June and July, the extent of the high-value Chl-a areas was relatively large, and concentrations were higher in the vicinity of the wind farm. After entering November and December, the overall Chl-a concentration decreased, and the extent of the high-value areas was reduced; however, relatively high concentration levels were still maintained within the wind farm and its adjacent waters. This is generally consistent with the seasonal pattern of "higher in summer and lower in winter" revealed by the remote-sensing and model-validation results.

The three-dimensional distribution results are shown in Fig. 12 (c).

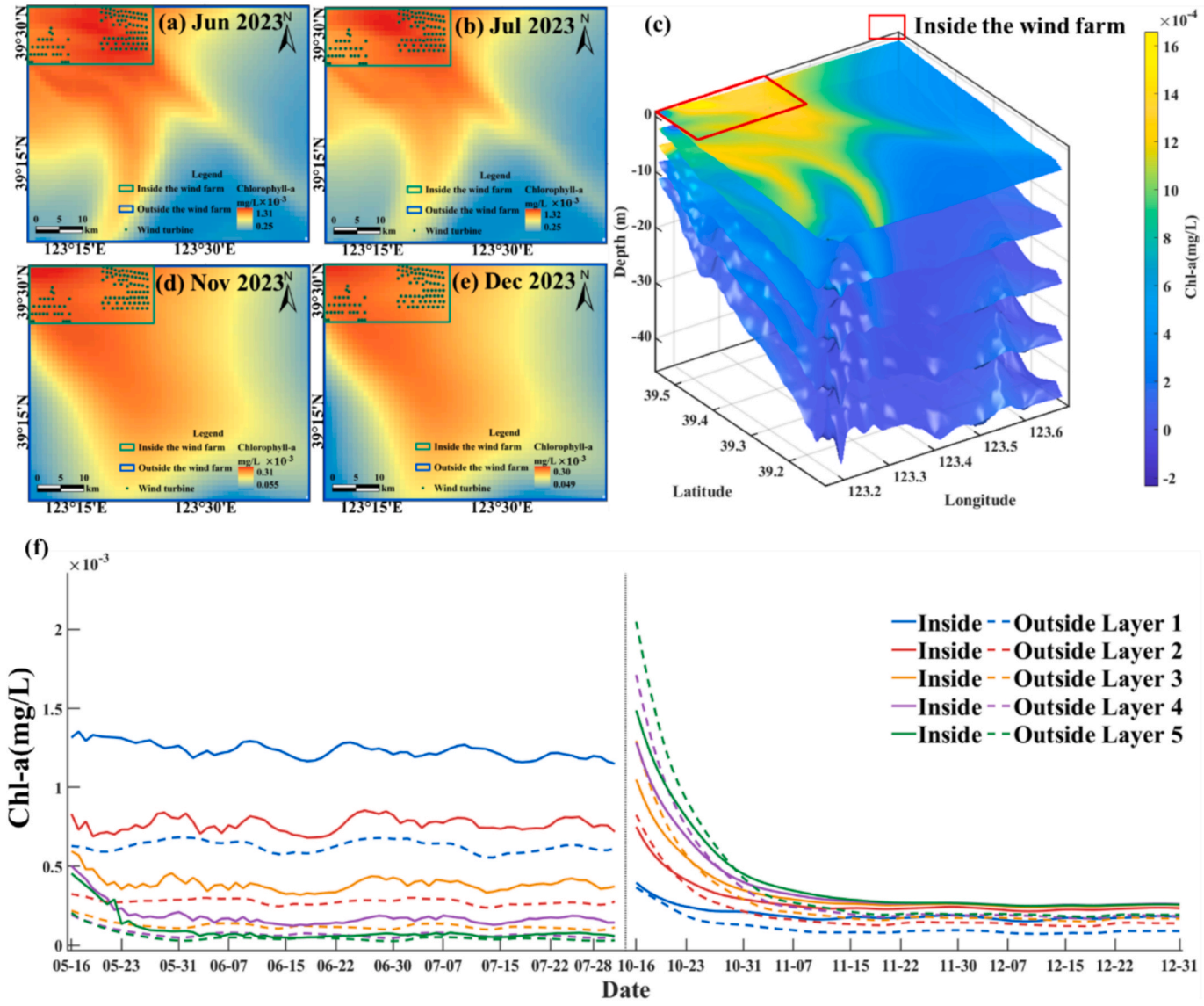

Fig. 12. Comparison of chlorophyll-a concentration inside and outside the wind farm.

Chl-a concentration exhibits clear vertical stratification, and the concentration differences among different water layers inside and outside the wind farm are relatively significant. Fig. 12 (f) further shows the temporal variation of Chl-a concentrations inside and outside the wind farm in different vertical layers. In summer, Chl-a concentrations both inside and outside the wind farm show obvious vertical stratification, generally decreasing with increasing water depth. At the same time, Chl-a concentrations in all layers inside the wind farm are generally higher than those outside, with the most obvious difference occurring in the surface layer, indicating a more pronounced accumulation of phytoplankton biomass inside the wind farm during summer. After entering winter, Chl-a concentration decreases rapidly at the beginning and then remains at a relatively low level overall, while the difference between the inside and outside of the wind farm becomes smaller than in summer.

The results in Fig. 12 indicate that the Chl-a concentrations simulated by the eutrophication model exhibit certain spatial differences in both the horizontal and vertical directions. Horizontally, Chl-a concentrations within the wind farm and its adjacent waters are generally higher than those in the surrounding region, which is broadly consistent with the spatial distribution characteristics revealed by the remote-sensing observations. Vertically, Chl-a concentrations are mainly concentrated in the upper water layers in summer and gradually decrease with increasing depth, whereas the vertical distribution pattern changes somewhat in winter. These results suggest that a certain degree of phytoplankton biomass accumulation may occur in the waters surrounding the wind farm and that this accumulation shows clear seasonal and vertical differences.

4.3.2. *Changes in dissolved oxygen*

Similarly, the numerical simulation results of DO from the eutrophication model for summer and winter 2023 were analyzed. Fig. 13 (a), 12 (b), 12 (d), and 12 (e) present the monthly mean DO concentrations for June, July, November, and December 2023, respectively, after applying Kriging interpolation to the results. The three-dimensional concentration distribution inside and outside the wind farm is depicted in Fig. 13 (c), and the concentration variation with depth over time is shown in Fig. 13 (f).

In terms of seasonal variation, DO concentrations were generally slightly higher in winter than in summer. In June and July, the DO concentrations in the study area were relatively low, whereas after entering November and December, the overall DO concentrations increased. This variation pattern differs somewhat from that of PC and Chl-a, with DO showing relatively lower values in summer and higher

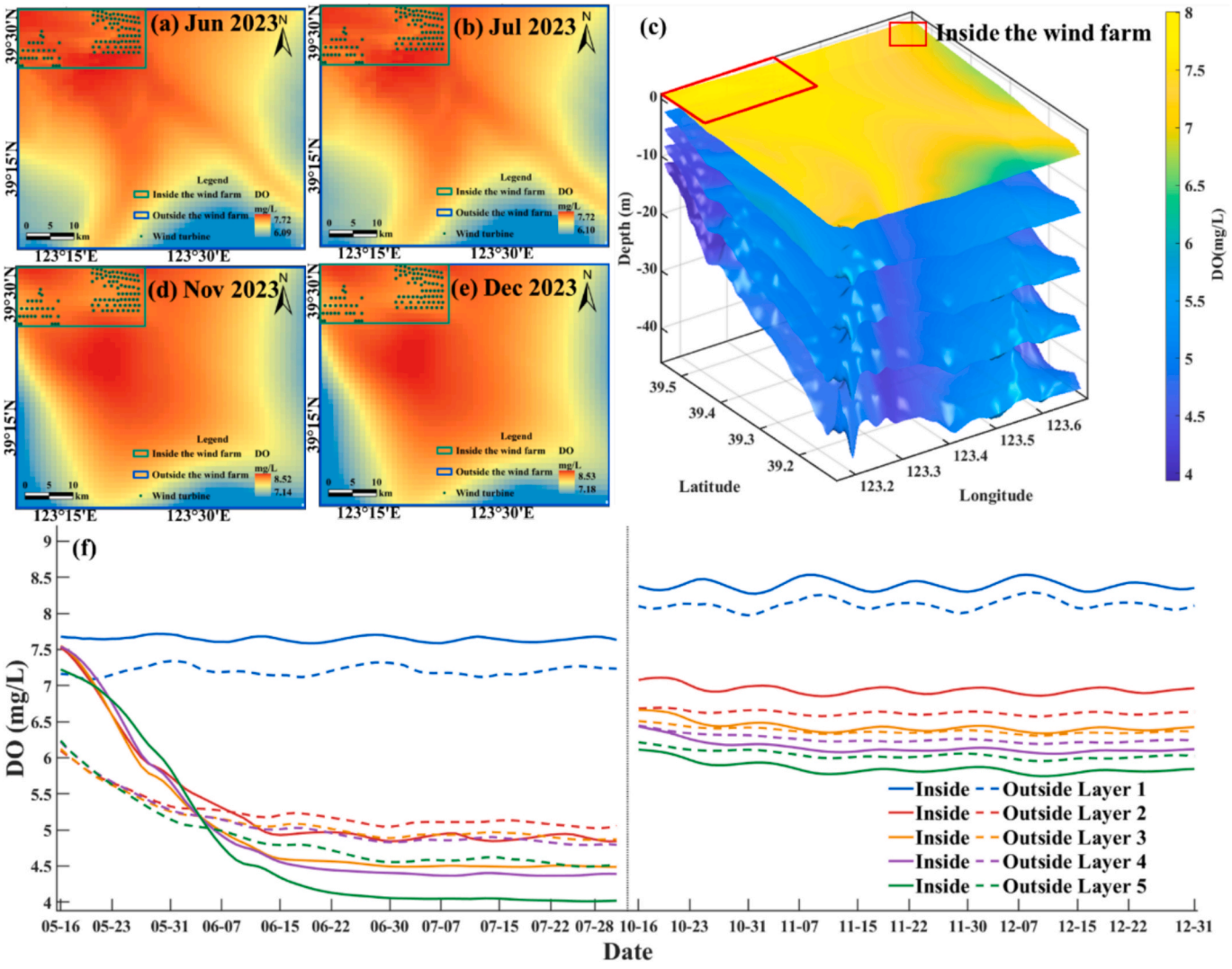

Fig. 13. Comparison of dissolved oxygen concentration inside and outside the wind farm.

values in winter.

The three-dimensional distribution results are shown in Fig. 13 (c). DO concentration exhibits clear vertical stratification, with generally higher values in the surface layer and a gradual decrease with increasing water depth. Fig. 13 (f) further shows the temporal variation of DO concentrations inside and outside the wind farm at different vertical layers. In summer, the surface-layer DO concentration is relatively high, and the surface DO concentration inside the wind farm is generally higher than that outside. As water depth increases, DO concentration decreases significantly. After entering winter, DO concentrations in all layers increase overall and remain relatively stable, while the difference between the inside and outside of the wind farm becomes smaller than in summer, although clear differences among vertical layers still exist.

The results in Fig. 13 indicate that the difference in DO concentration between the inside and outside of the wind farm is relatively weak at the horizontal scale, but certain differences are still observed at the local horizontal and vertical scales. Overall, DO concentration decreases with increasing water depth, and is higher in winter than in summer, indicating that its distribution is jointly influenced by seasonal variation and the vertical structure of the water column.

4.3.3. Changes in inorganic nitrogen and inorganic phosphorus

IN and IP are nutrients in water quality that play a vital role in promoting the proliferation of phytoplankton. Nutrients can lead to eutrophication, causing excessive phytoplankton growth. We analyzed the IN results from the eutrophication model's numerical simulations for summer and winter 2023. Fig. 14 (a), 13 (b), 13 (d), and 13 (e) present the monthly mean IN concentrations for June, July, November, and December 2023, respectively, after applying Kriging interpolation. The three-dimensional distribution of IN concentration inside and outside the wind farm is shown in Fig. 14 (c), and the temporal variation of concentration with depth is shown in Fig. 14 (f). The three-dimensional concentration distribution inside and outside the wind farm is shown in Fig. 14 (c), and the variation in concentration with depth over time is presented in Fig. 14 (f).

In terms of seasonal variation, IN concentrations were generally higher in summer than in winter, indicating a certain degree of seasonal difference. In summer, relatively high IN concentrations were maintained in the vicinity of the wind farm and in the western part of the study area. After entering winter, the overall IN concentration decreased, and the extent of the high-value areas was reduced; however, the waters adjacent to the wind farm still maintained relatively high levels.

As shown in Fig. 14 (c), IN concentration exhibits a vertical distribution pattern different from those of PC, Chl-a, and DO. Overall, the highest IN concentration does not occur in the surface layer; instead, it gradually increases with water depth, and the IN concentration in deeper water is clearly higher than that in surface water. This indicates

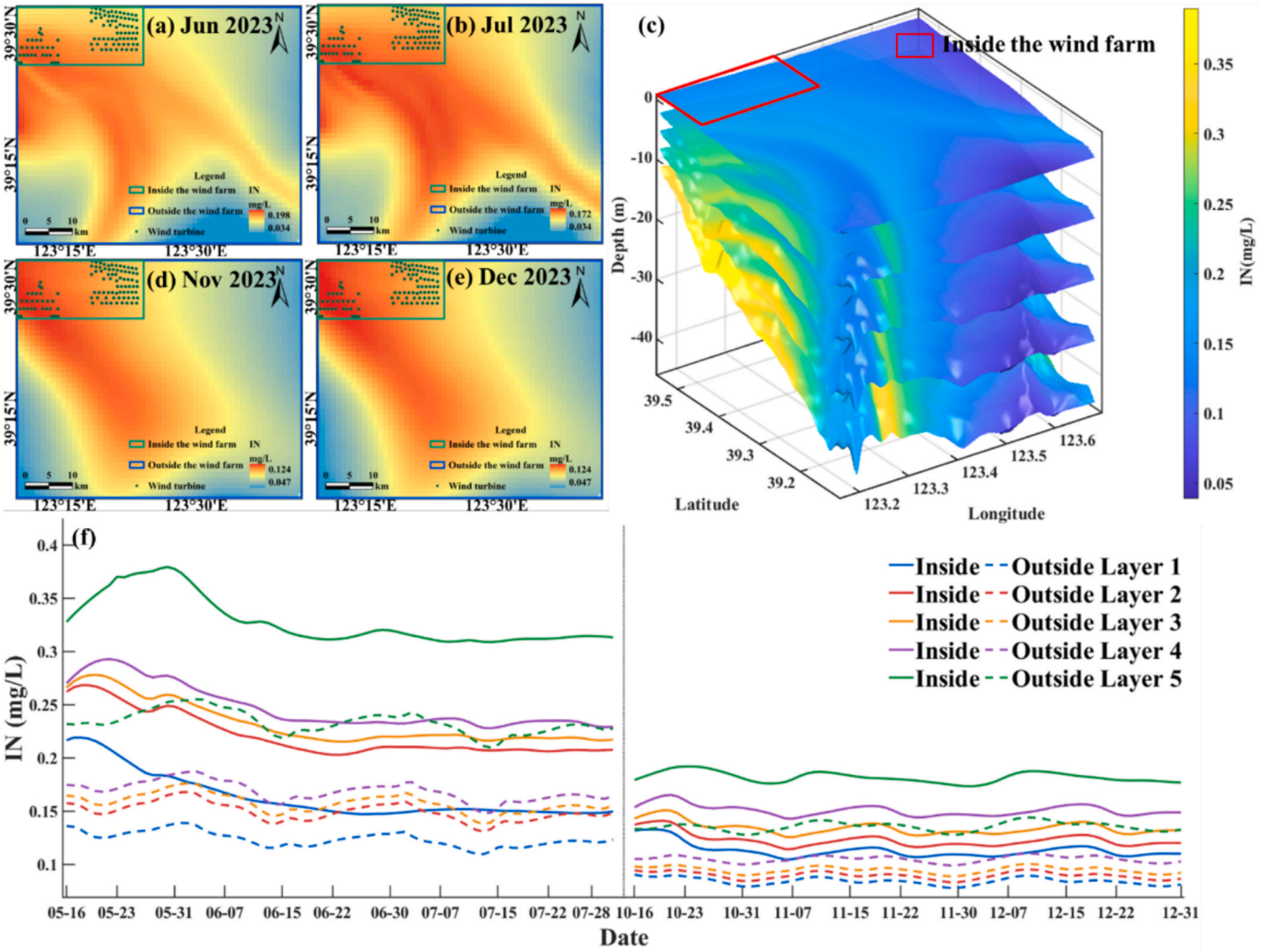

Fig. 14. Changes in inorganic nitrogen inside and outside the wind farm.

that IN has a strong vertical stratification, which may be related to phytoplankton uptake and consumption in the surface layer, nutrient accumulation in deeper water, and vertical exchange processes.

Fig. 14 (f) further shows the temporal variation of IN concentrations inside and outside the wind farm at different vertical layers. During the period from May to July, IN concentrations in all layers fluctuate to some extent, with the highest concentrations occurring in the deep layers and the lowest in the surface layer. The IN concentrations in all layers inside the wind farm are generally higher than those outside, with the differences being more obvious in the middle and lower layers. After entering October to December, the overall IN concentration decreases and the temporal variation becomes smaller, but the concentrations inside the wind farm remain generally higher than those in the surrounding waters.

Overall, IN concentrations around the wind farm show clear differences in both the horizontal and vertical directions. Horizontally, IN concentrations within the wind farm and its adjacent waters are relatively high. Vertically, IN concentration increases with water depth, with deeper water layers forming the main high-value zone. Unlike PC and Chl-a, which are mainly concentrated in the surface layer, IN shows a more obvious accumulation in deeper water, indicating that nutrient distribution around the wind farm may be jointly influenced by biological uptake, vertical mixing, and local hydrodynamic processes.

Similarly, we analyzed the IP results from the eutrophication model's numerical simulations for summer and winter 2023. Fig. 15 (a), 14 (b), 14 (d), and 14 (e) present the monthly mean IP concentrations for June, July, November, and December 2023, respectively, after applying Kriging interpolation. The three-dimensional concentration distribution inside and outside the wind farm is shown in Fig. 15 (c), and the variation in concentration with depth over time is presented in Fig. 15 (f).

In terms of seasonal variation, IP concentrations were generally higher in summer than in November and December. During summer, IP concentrations in the study area were relatively high, and the extent of the high-value areas was relatively large. After entering winter, the overall IP concentration decreased, and the extent of the high-value areas was reduced; however, the waters adjacent to the wind farm still maintained relatively high levels.

From the three-dimensional distribution results, IP concentration exhibits a clear vertical stratification. Unlike PC and Chl-a, which are mainly concentrated in surface layer, IP concentration generally increases with water depth, and the concentration in deeper water is significantly higher than that in the surface water. This suggests that surface IP may be maintained at a relatively low level due to phytoplankton uptake, whereas the middle and lower water layers show a more obvious pattern of nutrient accumulation.

The time-series results further indicate significant differences in IP concentration among different water layers. In summer, the highest IP concentrations occur in the deep-water layers, while the lowest occur in the surface layer, and the concentrations in most layers inside the wind farm are higher than those outside. After entering winter, IP concentrations in all layers decrease overall, and the magnitude of temporal variation becomes smaller, but the concentrations inside the wind farm

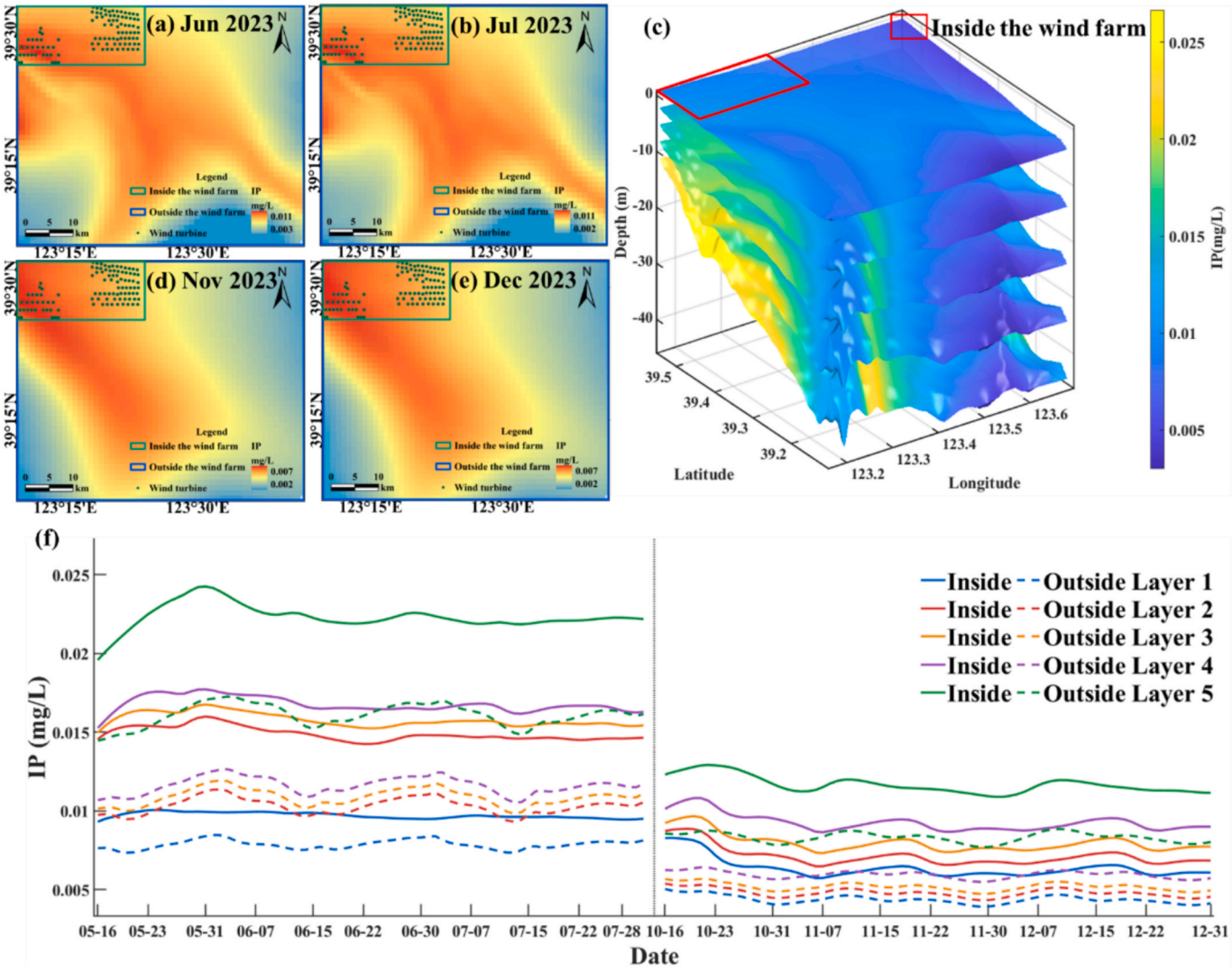

Fig. 15. Comparison of inorganic phosphorus inside and outside the wind farm.

remain generally higher than those in the surrounding waters.

These results indicate that IP concentrations around the wind farm show certain differences in both the horizontal and vertical directions. Horizontally, IP concentrations within the wind farm and its adjacent waters are relatively high. Vertically, IP concentration increases with water depth, with deeper water layers forming the main high-value zone. This distribution pattern is similar to that of IN, indicating that nutrient distribution around the wind farm is influenced not only by horizontal transport but also by closely related to vertical mixing, biological uptake, and nutrient accumulation in the middle and lower water layers.

4.4. Phytoplankton carbon and water-quality differences inside and outside the wind farm

We integrated the monthly mean values of PC and the major water-quality indicators across different vertical layers inside and outside the wind farm, and comparatively analyzed their concentration structures and relative differences in different months and water layers, as shown in the figure. In the figure, each month contains two stacked bars, representing the outside and inside regions of the wind farm, respectively. Different colors indicate different water layers. The percentages above the bars represent the relative rate of change inside the wind farm compared with the outside region. Positive values indicate that the concentration inside the wind farm is higher than that outside, whereas negative values indicate that the concentration inside the wind farm is lower than that outside.

As shown in Fig. 6 (a), PC concentrations inside the wind farm are generally significantly higher than those outside. In summer, the seasonal mean PC concentration inside the wind farm was approximately 2.5 times that outside, indicating a clear accumulation of PC within the wind farm during this season. In winter, the difference between the inside and outside decreases, but PC concentrations inside the wind farm remain higher, with the seasonal mean concentration being approximately 1.5 times that outside. Compared with summer, the increase in PC concentration in winter is clearly smaller, suggesting that the accumulation effect of PC inside the wind farm is more pronounced in summer. It is worth noting that PC concentrations in some water layers are relatively high in winter, which may be related to enhanced vertical mixing, particle settling and accumulation, and the relative enrichment of PC in bottom waters.

As shown in Fig. 16 (b), the variation pattern of Chl-a is generally similar to that of PC. In summer, Chl-a concentrations inside the wind farm are significantly higher than those outside, with the seasonal mean concentration inside the wind farm being approximately 2.3 times that outside, indicating higher phytoplankton biomass inside the wind farm during summer. In winter, the difference between the inside and outside generally decreases. In October, the Chl-a concentration inside the wind

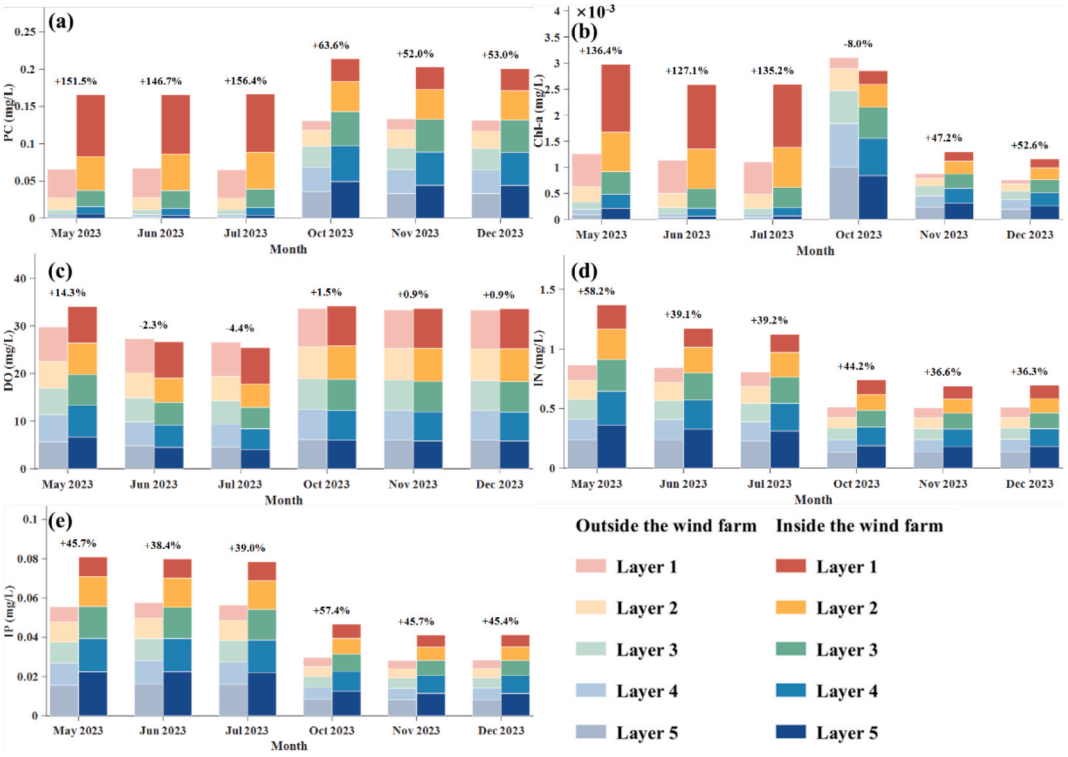

Fig. 16. Stacked comparison of phytoplankton carbon and water quality inside and outside the wind farm.

farm is slightly lower than that outside, with a relative change rate of -8.0%; in November and December, Chl-a concentrations inside the wind farm become higher again, with relative increases of 47.2% and 52.6%, respectively. Overall, the seasonal mean Chl-a concentration inside the wind farm remained higher than that outside in winter, being approximately 1.1 times that outside. This indicates that the difference in Chl-a between the inside and outside of the wind farm shows certain seasonal fluctuations, and its winter variation is more complex than that of PC. The lower concentration inside the wind farm in October may be related to model-result fluctuations and spatial errors introduced during the Kriging interpolation process.

As shown in Fig. 16 (c), the difference in DO concentration between the inside and outside of the wind farm is relatively weak. In May, the DO concentration inside the wind farm is higher than that outside, with a relative increase of approximately 14.3%. In June and July, the DO concentration inside the wind farm is slightly lower than that outside, with relative change rates of −2.3% and −4.4%, respectively. After entering winter, the difference in DO concentration between the inside and outside further decreases, showing only slight increases of about 0.9%–1.5%. Overall, the seasonal mean DO concentration inside the wind farm was approximately 2.93% higher than that outside in summer and 1.12% higher in winter. Compared with PC and Chl-a, the difference in DO concentration between the inside and outside of the wind farm is not significant, and the overall variation is relatively stable.

As shown in Fig. 16 (d), IN concentrations inside the wind farm are generally higher than those outside. In summer, the seasonal mean IN concentration inside the wind farm was approximately 45.72% higher than that outside; in winter, it was approximately 39.04% higher. This indicates that IN inside the wind farm shows a certain degree of enrichment in both summer and winter, and that the difference between the inside and outside is relatively stable.

As shown in Fig. 16 (e), IP concentrations also remain higher inside the wind farm than outside. In summer, the seasonal mean IP concentration inside the wind farm was approximately 41.00% higher than that outside; in winter, it was approximately 49.59% higher. Similar to IN, IP shows a relatively stable enrichment pattern inside the wind farm, indicating that nutrient concentrations inside the wind farm are generally higher than those outside.

Overall, the results shown in the figure indicate clear differences in the multilayer concentration structures of water-quality indicators between the inside and outside of the wind farm. Among them, the differences in PC and Chl-a are the most pronounced, especially during the summer period from May to July, when the increases inside the wind farm relative to the outside region are particularly large, indicating a clear accumulation of phytoplankton-related indicators within the wind farm. IN and IP also show relatively stable enrichment inside the wind farm, suggesting that the wind-farm structures may have a certain influence on the spatial distribution of nutrients in the surrounding waters. In contrast, the difference in DO concentration between the inside and outside of the wind farm is relatively small, and its overall variation is comparatively stable. Taken together, offshore wind farm have a more pronounced influence on PC, Chl-a, and nutrient concentrations, among which PC and Chl-a show the largest variations, and these effects are more evident in summer.

5. Discussion

5.1. Combining remote sensing and numerical simulations benefits

The combination of remote sensing and numerical simulations has demonstrated unique advantages in environmental monitoring and ecological research. Firstly, numerical simulations (He et al., 2024) typically rely on extensive field data, which often need to be obtained through ground observations and experiments. The data collection process is time-consuming and costly (Luo et al., 2021). In contrast, remote sensing technology, through satellite and airborne platforms (McCarthy et al., 2025), can efficiently and rapidly collect environmental data over large areas, significantly reducing the need for data collection. Remote sensing enables real-time monitoring of environmental changes over vast regions, making it particularly suitable for large-scale assessments and providing strong data support for numerical simulations.

Secondly, remote sensing data offer broad spatial coverage (Kaplan et al., 2024), but tend to provide weaker descriptions at the detailed level. In contrast, numerical simulations allow for high-precision analysis and predictions within localized areas, offering more detailed descriptions. Through numerical simulations, it is possible to gain a deeper understanding of dynamic changes within wind farms or other specific regions, revealing micro-scale processes that remote sensing data may not capture.

The combination of remote sensing and numerical simulations not only enhances research efficiency and data accuracy but also provides a multi-scale analytical framework for environmental impact assessments of offshore wind farms. Through the synergistic use of remote sensing and numerical simulations, a more comprehensive and precise understanding of the impacts of offshore wind farms on water bodies can be achieved, promoting the continued development of the offshore wind energy industry.

5.2. Analysis of the causes of differences inside and outside the wind farm

(Lindeboom et al., 2011) have also shown that water flow direction and velocity affect PC concentration and water quality (Wang et al., 2024). To further identify the potential hydrodynamic mechanisms driving the differences between the inside and outside of the wind farm, this study used the U and V velocity components derived from the hydrodynamic model to calculate the mean vector flow fields for summer (Fig. 17 (c)) and winter (Fig. 17 (d)), respectively. These were then overlaid with the spatial distribution of PC concentration for comparative analysis, as shown in Fig. 17.

The results show that the overall water flow in the study area exhibited a transport pattern toward the west or northwest in both summer and winter. By comparison, the flow direction was more consistent in summer, whereas the overall flow pattern was less coherent in winter. This difference may be one of the reasons why larger differences in PC and Chl-a concentrations were observed between the inside and outside of the wind farm during summer.

The specific effects are shown in Fig. 17 (a) and 17 (b). In the outer region of the wind farm, the flow direction is generally continuous, whereas within the wind farm and around the turbines, local deflections of the flow direction occur. The turbine structures and array layout may weaken water exchange between the interior of the wind farm and the surrounding waters, thereby forming relatively low-velocity wake zones downstream of the turbines. This process is conducive to the retention and accumulation of phytoplankton and nutrients in areas with weaker hydrodynamic disturbance, which in turn promotes an increase in PC concentration within the wind farm (Austin et al., 2025; Gunn and Stock-Williams, 2013; Rennau et al., 2012).

5.3. Phytoplankton carbon-water quality relationship

To further explore the potential factors contributing to the increase in PC concentration within the offshore wind farm, we conducted a correlation analysis based on the differences in water-quality indicators between the inside and outside of the wind farm (Fig. 18). Considering that turbine foundations and array structures may alter local hydrodynamic conditions, weaken water exchange, and promote the retention and accumulation of phytoplankton and nutrients, the differences in PC, Chl-a, DO, IN, and IP between the inside and outside of the wind farm were calculated, where positive values indicate higher concentrations inside the wind farm and negative values indicate the opposite.

The correlation results show that the difference in PC is very strongly positively correlated with the difference in Chl-a ($r = 0.99$), indicating that the increase in PC inside the wind farm is closely related to an increase in phytoplankton biomass. The difference in PC is also significantly positively correlated with the difference in DO ($r = 0.93$), suggesting that the increase in PC may be accompanied by enhanced photosynthesis and elevated DO levels. In terms of nutrients, the difference in PC shows a moderate positive correlation with the difference in IN ($r = 0.52$), indicating that IN enrichment may provide nutritional support for phytoplankton growth, whereas the correlation between the differences in PC and IP is very weak ($r \approx 0$), suggesting that IP is not a

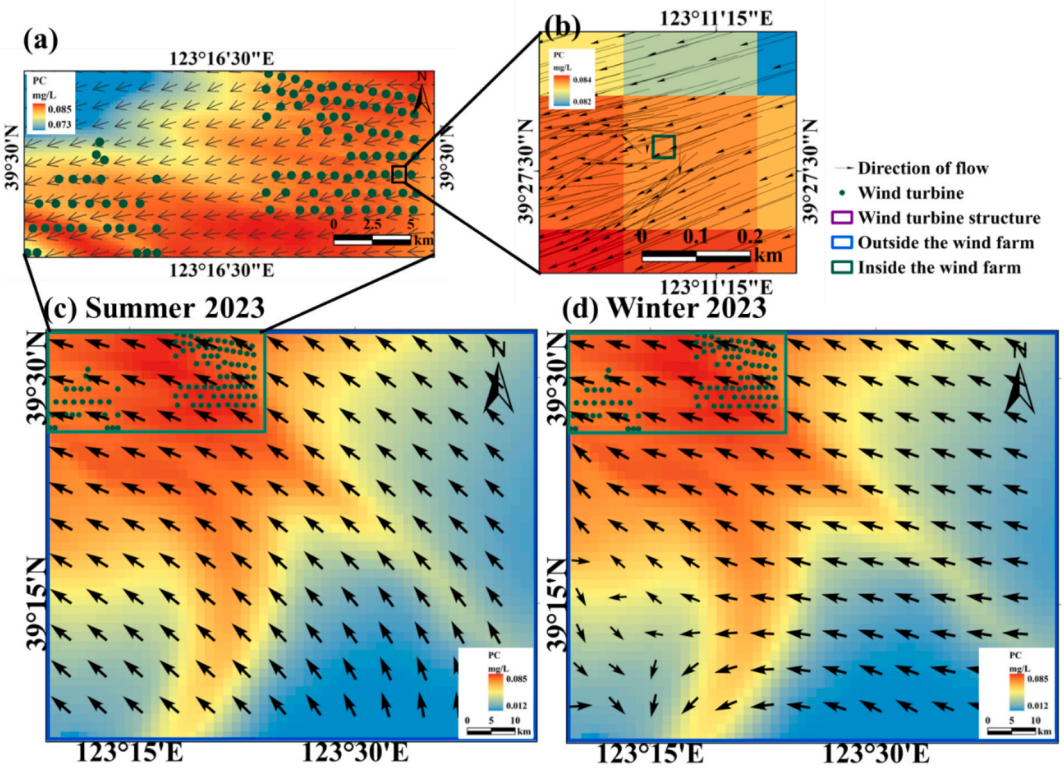

Fig. 17. Water flow direction and phytoplankton carbon concentration on June 1, 2023.

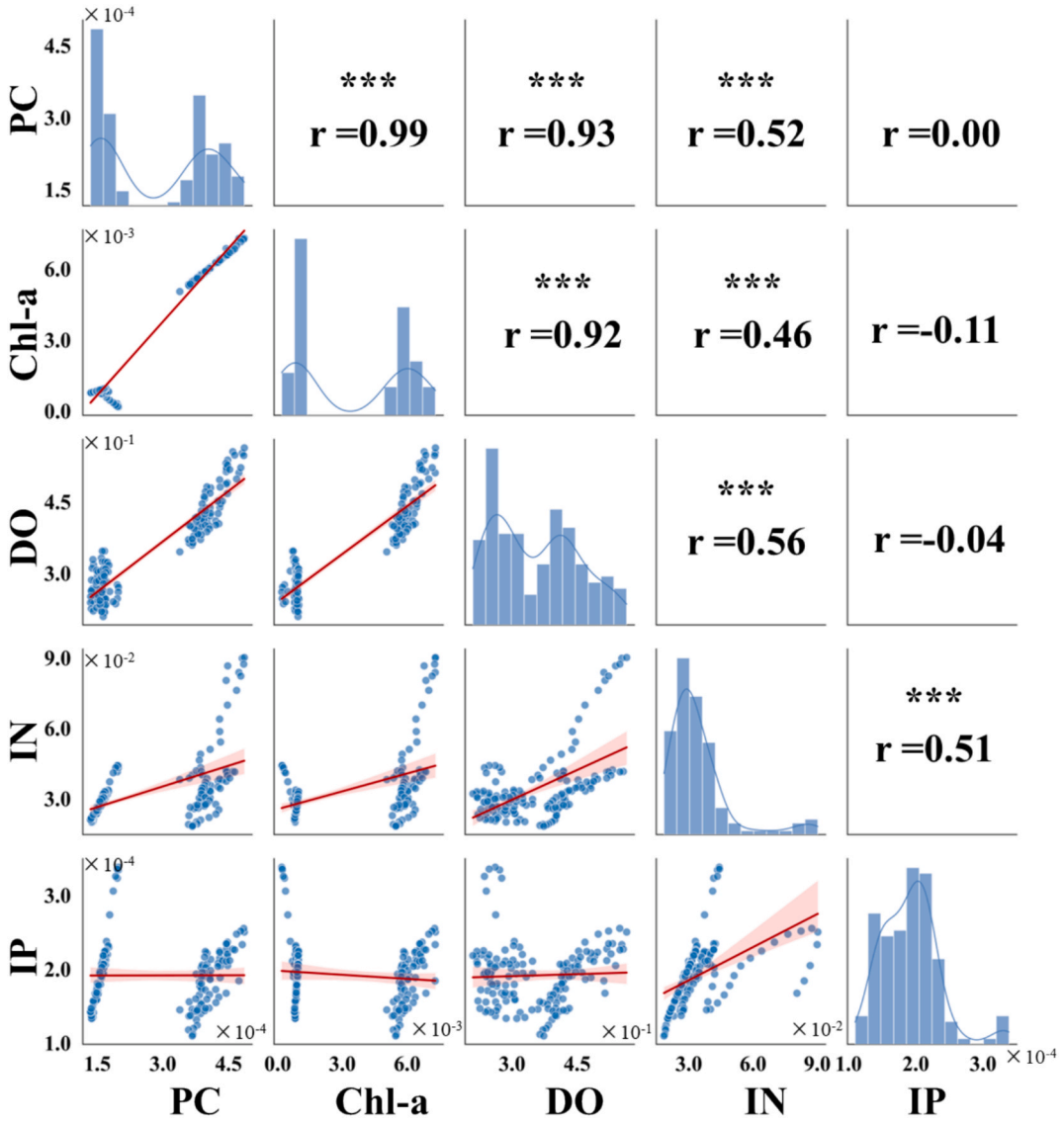

Fig. 18. Comparison of the correlation between phytoplankton carbon concentration and water quality (* indicates $0.01 \leq p < 0.05$, ** indicates $0.001 \leq p < 0.01$, *** indicates $p < 0.001$).

major direct factor explaining the inside–outside difference in PC. In addition, the difference in IN is significantly positively correlated with the difference in IP, indicating synchronous nutrient variation inside the wind farm; however, their influence on PC may be jointly regulated by nutrient limitation, differential uptake, or hydrodynamic retention.

Overall, the increase in PC inside the wind farm is most closely related to the inside–outside differences in Chl-a and DO, indicating that increased phytoplankton biomass and enhanced photosynthesis are important manifestations of the PC increase. The positive correlation with IN further supports the role of nutrient enrichment. Combined with the flow-field analysis, the offshore wind-farm structures may promote the accumulation of PC, Chl-a, and related water-quality indicators inside the wind farm by altering local hydrodynamic conditions, reducing water exchange intensity, and enhancing material retention. It should be noted that correlation analysis only reveals statistical relationships and cannot by itself prove causality, but it provides important evidence for explaining the potential mechanisms underlying the elevated PC concentration inside the wind farm.

Research by (Hunter and Laws, 2003) demonstrated a significant positive correlation between Chl-a and PC concentrations. As Chl-a concentration increases, PC accumulation typically shows an upward trend, reflecting enhanced photosynthetic activity and increased phytoplankton biomass. (Behrenfeld and Falkowski, 2003) explained that during photosynthesis, phytoplankton absorb carbon dioxide from the water and convert it into organic matter, with oxygen being released as a byproduct. The higher the PC concentration, the stronger the photosynthetic activity, leading to an increase in DO concentration. This explains the significant correlation between PC concentration and DO. Studies by (Coolen et al., 2022) and (Liu, Jiang, et al., 2024) have shown that changes in nutrients such as IN and IP can indeed affect phytoplankton community dynamics. However, according to the comparison results in Fig. 18, nutrient variation may play a certain promoting role in the increase in PC concentration within the wind farm, but it is not the primary cause of the differences between the inside and outside of the wind farm. In contrast, the offshore wind-farm structures are more likely to alter local hydrodynamic conditions, reduce water exchange intensity, and potentially generate an artificial reef effect (Chong et al., 2023), thereby enhancing material retention and local accumulation, which may ultimately lead to overall higher PC and related water-quality indicators inside the wind farm than in the surrounding outer region.

5.4. Implications for adaptation and mitigation

Our results indicate that the impacts of offshore wind farms on PC and water-quality indicators show clear spatiotemporal heterogeneity, and their responses vary with season, water-column structure, and local hydrodynamic conditions. In particular, the differences in PC and Chl-a between the inside and outside of the wind farm are more pronounced in summer, which may be related to stronger biological activity in this season and to the greater tendency for turbine-array-induced disturbances of the local flow field to be translated into material retention and accumulation. Therefore, in the siting and ecological-environmental management of offshore wind farms (Zhao et al., 2022), in addition to considering their benefits for renewable-energy development, it is also necessary to incorporate ecological impacts into adaptation- and mitigation-related management frameworks (Galparsoro et al., 2022). Specifically, during the planning stage, ecologically sensitive marine areas may be prioritized for avoidance, and siting optimization can be carried out by considering local hydrodynamic conditions and seasonal ecological characteristics. (Rezaei et al., 2023) During the operational stage, long-term ecological monitoring in key seasons both inside and outside the wind farm may be strengthened, with particular attention to the coupled variations of PC, Chl-a, nutrients, and hydrodynamic indicators. At the management level, zoned monitoring and dynamic assessment mechanisms based on multiple temporal and spatial scales may be established, and surrounding fishing-use areas and coastal communities may be incorporated into risk identification and adaptive management to improve the relevance and regional applicability of management measures.

5.5. Uncertainty and perspectives

This study mainly focused on the effects of offshore wind farms on regional-scale hydrodynamic processes and water quality, rather than resolving hydrodynamic processes around individual wind turbines. Therefore, this study treated offshore wind turbines as impermeable solid boundaries that did not participate in water exchange and equivalently treated them as no-flow boundaries in the model. Although this simplification could generally evaluate the effects of offshore wind turbines on water exchange and material transport, we did not consider the high-frequency turbulence, wake vortices, and local vertical mixing processes around individual wind turbines (Austin et al., 2025; Cazenave et al., 2016; Hendriks et al., 2025; Hosseini et al., 2025). Therefore, if the purpose of researchers is to evaluate the effects of individual wind turbines on hydrodynamic processes and water quality, the above processes need to be considered, and more refined numerical models should be used for simulation.

In addition, the wind turbines in our study area were impermeable monopile structures, and the simulation process in this paper was not applicable to permeable multi-pile structures or floating offshore wind turbines. More complex interactions exist between the mooring systems of multi-pile structures and floating wind turbines and the surrounding water bodies, and wind turbines should not be simply simplified as no-flow boundaries. Instead, simulations should be conducted by considering the specific wind turbine types, structural characteristics of wind turbines, and local hydrodynamic conditions (Wang, Cai, et al., 2023; Zeng et al., 2024).

In addition, in this study, we used MODIS-based PC and Chl-a data. Previous studies have demonstrated the reliability and applicability of these products (Bailey and Werdell, 2006; Behrenfeld et al., 2005; Graff et al., 2015), and these data had good spatial-scale matching with the numerical simulation results in this study. However, a single remote-sensing data source may still lead to errors being propagated from imagery to the numerical simulation process (Tilstone et al., 2021). In future studies, multi-source satellite remote-sensing products can be considered as inputs for numerical models, and the robustness of numerical simulation under different remote-sensing data sources can be compared to improve the reliability of assessing the effects of offshore wind farms on PC and water quality.

6. Conclusion

In this study, we fully leverage the advantages of remote sensing technology in data collection, enabling the rapid and efficient acquisition of large-scale PC concentration and Chl-a concentration data. These remote sensing data are used to establish the initial values and boundary conditions in the numerical simulation models, ensuring the accuracy of the simulation's driving forces and boundary conditions. Additionally, the remote sensing data play a role in cross-validation of the numerical simulation results. By comparing the differences between simulated and remote sensing observations, the reliability and predictive capability of the numerical simulation are further verified. This integration allows for a more accurate assessment of the impact of wind farms on PC concentration and water quality.

Both the remote-sensing retrievals and the model simulations indicate that PC and Chl-a concentrations within the wind farm and its adjacent waters are generally higher than those in the surrounding outer region, suggesting that a certain degree of phytoplankton accumulation may occur around the wind farm. This feature shows clear seasonality, with the most pronounced effect occurring in summer. From May to July, the PC and Chl-a concentrations inside the wind farm are significantly higher than those outside. In winter, both concentrations decrease overall, and the difference between the inside and outside of the wind farm becomes smaller, although the concentrations inside the wind farm remain relatively higher. The three-dimensional simulation results further indicate that this difference is not only reflected in the surface water but also shows certain variations in the vertical distribution. In contrast, the horizontal difference in DO between the inside and outside of the wind farm is relatively weak, whereas IN and IP show a certain degree of accumulation inside the wind farm, suggesting that the wind farm may have a certain influence on the spatial distribution of nutrients.

We further used correlation analysis and hydrodynamic results to reveal the potential mechanisms underlying the differences between the inside and outside of the wind farm. The difference in PC is most closely related to the differences in Chl-a and DO, indicating that the increase in PC inside the wind farm is associated with increased phytoplankton biomass and enhanced photosynthesis. The positive correlation between PC and IN suggests that IN enrichment may provide certain nutritional support for phytoplankton growth. Meanwhile, the hydrodynamic analysis shows that turbine foundations and array structures can disturb the local flow field, causing deflection of the flow direction inside the wind farm and around the turbines, and may weaken water exchange between the interior of the wind farm and the surrounding waters. Such local low-velocity zones and wake zones are conducive to the retention and accumulation of phytoplankton and some nutrients, thereby further promoting the increase of PC, Chl-a, and nutrient concentrations inside the wind farm.

There are also some limitations in our study. Due to the constraints of the numerical simulation duration (Zheng et al., 2024), we only simulated the changes in PC concentration during the peak growth season of surface algae. Although this approach is commonly adopted (Huggett et al., 2021), investigating the seasonal variations in PC concentration and water quality would be meaningful. Additionally, we aim to extend our research beyond the five parameters—PC, Chl-a, DO, IN, and IP—and will conduct further studies on other impacts of offshore wind farms.

CRediT authorship contribution statement

Xinglong Guo: Writing – original draft, Software, Data curation. **Guoqing Li:** Writing – review & editing, Methodology, Conceptualization. **Hongyuan Shi:** Validation, Methodology, Conceptualization.

Lingrui Guo: Validation, Project administration. **Jing Yu:** Software, Investigation.

Declaration of competing interest

The authors declare that they have no known competing financial interests or personal relationships that could have appeared to influence the work reported in this paper.

Acknowledgments

This research received financial support from the National Natural Science Fund of China (42271266), Innovation Project for graduate students of Ludong University (IPGS 2024-067, IPGS 2024-068).

Data availability

Data will be made available on request.

References

Abhishek, Kinouchi, T., 2021. Synergetic application of GRACE gravity data, global hydrological model, and in-situ observations to quantify water storage dynamics over Peninsular India during 2002–2017. J. Hydrol. 596. https://doi.org/10.1016/j.jhydrol.2021.126069.

Abhishek, Kinouchi, T., Sayama, T., 2021. A comprehensive assessment of water storage dynamics and hydroclimatic extremes in the Chao Phraya River Basin during 2002–2020. J. Hydrol. 603. https://doi.org/10.1016/j.jhydrol.2021.126868.

Austin, M.J., Unsworth, C.A., Van Landeghem, K.J.J., Lincoln, B.J., 2025. Enhanced bed shear stress and mixing in the tidal wake of an offshore wind turbine monopile. Ocean Sci. 21 (1), 81–91. https://doi.org/10.5194/os-21-81-2025.

Bailey, H., Brookes, K., Thompson, P., 2014. Assessing environmental impacts of offshore wind farms: lessons learned and recommendations for the future. Aquat. Biosyst. 10, 8. https://doi.org/10.1186/2046-9063-10-8.

Bailey, S.W., Werdell, P.J., 2006. A multi-sensor approach for the on-orbit validation of ocean color satellite data products. Remote Sens. Environ. 102 (1–2), 12–23. https://doi.org/10.1016/j.rse.2006.01.015.

Behrenfeld, M.J., Boss, E., Siegel, D.A., Shea, D.M., 2005. Carbon-based ocean productivity and phytoplankton physiology from space. Global Biogeochem. Cycles 19 (1). https://doi.org/10.1029/2004GB002299.

Behrenfeld, M.J., Falkowski, P.G., 2003. Photosynthetic rates derived from satellite-based chlorophyll concentration. Limnol. Oceanogr. 42 (1), 1–20. https://doi.org/10.4319/lo.1997.42.1.0001.

Bergström, L., Kautsky, L., Malm, T., Rosenberg, R., Wahlberg, M., Åstrand Capetillo, N., Wilhelmsson, D., 2014. Effects of offshore wind farms on marine wildlife—a generalized impact assessment. Environ. Res. Lett. 9 (3). https://doi.org/10.1088/1748-9326/9/3/034012.

Bijma, J., Portner, H.O., Yesson, C., Rogers, A.D., 2013. Climate change and the oceans–what does the future hold? Mar. Pollut. Bull. 74 (2), 495–505. https://doi.org/10.1016/j.marpolbul.2013.07.022.

Cazenave, P.W., Torres, R., Allen, J.I., 2016. Unstructured grid modelling of offshore wind farm impacts on seasonally stratified shelf seas. Prog. Oceanogr. 145, 25–41. https://doi.org/10.1016/j.pocean.2016.04.004.

Chen, Y., Lin, H., 2022. Overview of the development of offshore wind power generation in China. Sustain. Energy Technol. Assess. 53. https://doi.org/10.1016/j.seta.2022.102766.

Chong, L., Siders, Z.A., Lorenzen, K., Ahrens, R.N.M., Camp, E.V., 2023. Global synthesis of effects and feedbacks from artificial reefs on socioecological systems in recreational fisheries. Fish Fish. 25 (2), 303–319. https://doi.org/10.1111/faf.12809.

Coolen, J.W.P., Vanaverbeke, J., Dannheim, J., Garcia, C., Birchenough, S.N.R., Krone, R., Beermann, J., 2022. Generalized changes of benthic communities after construction of wind farms in the southern North Sea. J. Environ. Manage. 315, 115173. https://doi.org/10.1016/j.jenvman.2022.115173.

De La Peña, L., Guo, R., Cao, X., Ni, X., Zhang, W., 2022. Accelerating the energy transition to achieve carbon neutrality. Resour. Conserv. Recycl. 177. https://doi.org/10.1016/j.resconrec.2021.105957.

Flindt, M.R., Kamp-Nielsen, L., 1997. Modelling of an estuarine eutrophication gradient. Ecol. Model. 102 (1), 143–153. https://doi.org/10.1016/S0304-3800 (97)00101-4.

Floeter, J., van Beusekom, J.E.E., Auch, D., Callies, U., Carpenter, J., Dudeck, T., et al., 2017. Pelagic effects of offshore wind farm foundations in the stratified North Sea. Prog. Oceanogr. 156, 154–173. https://doi.org/10.1016/j.pocean.2017.07.003.

Galparsoro, I., Menchaca, I., Garmendia, J.M., Borja, Á., Maldonado, A.D., Iglesias, G., Bald, J., 2022. Reviewing the ecological impacts of offshore wind farms. npj Ocean Sustainability 1 (1). https://doi.org/10.1038/s44183-022-00003-5.

Ganju, N.K., Brush, M.J., Rashleigh, B., Aretxabaleta, A.L., del Barrio, P., Grear, J.S., et al., 2015. Progress and challenges in coupled hydrodynamic-ecological estuarine modeling. Estuar. Coasts 39 (2), 311–332. https://doi.org/10.1007/s12237-015-0011-y.

Graff, J.R., Westberry, T.K., Milligan, A.J., Brown, M.B., Dall'Olmo, G., Dongen-Vogels, V.V., et al., 2015. Analytical phytoplankton carbon measurements spanning diverse ecosystems. Deep Sea Res. Part I 102, 16–25. https://doi.org/10.1016/j.dsr.2015.04.006.

Gunn, K., Stock-Williams, C., 2013. On validating numerical hydrodynamic models of complex tidal flow. Int. J. Mar. Energy 3–4, e82–e97. https://doi.org/10.1016/j.ijome.2013.11.013.

Guo, S., Zhang, Y., Zhang, X., Yang, Y., Cheng, W., 2025. Simulation study of reservoir water environment based on Mike21-taking Baisha reservoir as an example. Dyn. Atmos. Oceans 109. https://doi.org/10.1016/j.dynatmoce.2024.101522.

He, Y., Ou, G.Z., Zhang, Z., Shen, Z.T., Wei, H., Ding, X.H., et al., 2024. On-site monitoring and numerical simulation on groundwater flow and pollution plume evolution in a hexavalent-chromium contaminated site. J. Hazard. Mater. 479, 135662. https://doi.org/10.1016/j.jhazmat.2024.135662.

Hendriks, E., Langedock, K., van Duren, L.A., Vanaverbeke, J., Boone, W., Soetaert, K., 2025. The impact of offshore wind turbine foundations on local hydrodynamics and stratification in the Southern North Sea. Front. Mar. Sci. 12. https://doi.org/10.3389/fmars.2025.1619577.

Hong, Y., Liu, Z., Li, S., Long, Y., Gao, J., Hu, R., Ye, J., 2024. Benign water quality and phytoplankton status during the operation of Guishan offshore wind farm in the Pearl River Estuary, China. Regional Stud. Mar. Sci. 77. https://doi.org/10.1016/j.rsma.2024.103637.

Hosseini, S.T., Pein, J., Staneva, J., Zhang, Y.J., Stanev, E., 2025. Impact of offshore wind farm monopiles on hydrodynamics interacting with wind-driven waves. Ocean Model. 195, 102521. https://doi.org/10.1016/j.ocemod.2025.102521.

Hu, C., Feng, L., Lee, Z., Franz, B.A., Bailey, S.W., Werdell, P.J., Proctor, C.W., 2019. Improving satellite global chlorophyll a data products through algorithm refinement and data recovery. J. Geophys. Res. Oceans 124 (3), 1524–1543. https://doi.org/10.1029/2019jc014941.

Huggett, R.D., Haigh, I.D., Purdie, D.A., 2021. Modelling the impact of river flow, macronutrients and solar radiation on the eutrophication status of small shallow estuaries. J. Mar. Syst. 222. https://doi.org/10.1016/j.jmarsys.2021.103606.

Hunter, B.L., Laws, E.A., 2003. ATP and chlorophyll a as estimators of phytoplankton carbon biomass1. Limnol. Oceanogr. 26 (5), 944–956. https://doi.org/10.4319/lo.1981.26.5.0944.

Jia, H., Shen, Y., Su, M., Yu, C., 2018. Numerical simulation of hydrodynamic and water quality effects of shoreline changes in Bohai Bay. Front. Earth Sci. 12 (3), 625–639. https://doi.org/10.1007/s11707-018-0688-x.

Kaplan, G., Yalcinkaya, F., Altıok, E., Pietrelli, A., Nastro, R.A., Lovecchio, N., et al., 2024. The role of remote sensing in the evolution of water pollution detection and monitoring: a comprehensive review. Phys. Chem. Earth, Parts A/B/C 136. https://doi.org/10.1016/j.pce.2024.103712.

Kordan, M.B., Yakan, S.D., 2024. The effect of offshore wind farms on the variation of the phytoplankton population. Reg. Stud. Mar. Sci. 69. https://doi.org/10.1016/j.rsma.2023.103358.

Lecordier, E.M., Gernez, P., Mazik, K., York, K., Forster, R.M., 2025. Quantification of turbid wakes in offshore wind farms using satellite remote sensing. Sci. Total Environ. 967. https://doi.org/10.1016/j.scitotenv.2025.178814.

Li, J., Wang, G., Li, Z., Yang, S., Chong, W.T., Xiang, X., 2020. A review on development of offshore wind energy conversion system. Int. J. Energy Res. 44 (12), 9283–9297. https://doi.org/10.1002/er.5751.

Lindeboom, H.J., Kouwenhoven, H.J., Bergman, M.J.N., Bouma, S., Brasseur, S., Daan, R., et al., 2011. Short-term ecological effects of an offshore wind farm in the Dutch coastal zone; a compilation. Environ. Res. Lett. 6 (3). https://doi.org/10.1088/1748-9326/6/3/035101.

Liu, Q., Jiang, Y., Huang, X., Liu, Y., Guan, M., Tian, Y., 2024a. Hydrological conditions can change the effects of major nutrients and dissolved organic matter on phytoplankton community dynamics in a eutrophic river. J. Hydrol. 628. https://doi.org/10.1016/j.jhydrol.2023.130503.

Liu, Y., Mao, X., Shi, J., Luo, Y., Guo, X., Wang, Y., 2024b. Seasonal and spatial variations of dissolved inorganic nitrogen exchange between the Yellow Sea and the East China Sea and the influencing factors. Mar. Pollut. Bull. 208. https://doi.org/10.1016/j.marpolbul.2024.116992.

Lu, Z., Li, G., Liu, Z., Wang, L., 2022. Offshore wind farms changed the spatial distribution of chlorophyll-a on the sea surface. Front. Mar. Sci. 9. https://doi.org/10.3389/fmars.2022.1008005.

Luo, F., Gou, H., Li, R., Wang, H., Chen, Z., Lin, W., Li, K., 2021. Numerical simulation on marine environmental capacity in the open sea area of Northern Jiangsu Province using a three-dimensional water quality model based on FVCOM. Reg. Stud. Mar. Sci. 45. https://doi.org/10.1016/j.rsma.2021.101856.

McCarthy, M.J., Herrero, H.V., Insalaco, S.A., Hinten, M.T., Anyamba, A., 2025. Satellite remote sensing for environmental sustainable development goals: a review of applications for terrestrial and marine protected areas. Remote Sens. Appl.: Soc. Environ. 37. https://doi.org/10.1016/j.rsase.2025.101450.

Nunneri, C., Lenhart, H.J., Burkhard, B., Windhorst, W., 2008. Ecological risk as a tool for evaluating the effects of offshore wind farm construction in the North Sea. Reg. Environ. Chang. 8 (1), 31–43. https://doi.org/10.1007/s10113-008-0045-9.

Potrč, S., Čuček, L., Martin, M., Kravanja, Z., 2021. Sustainable renewable energy supply networks optimization – the gradual transition to a renewable energy system within the European Union by 2050. Renew. Sustain. Energy Rev. 146. https://doi.org/10.1016/j.rser.2021.111186.

Rennau, H., Schimmels, S., Burchard, H., 2012. On the effect of structure-induced resistance and mixing on inflows into the Baltic Sea: a numerical model study. Coast. Eng. 60, 53–68. https://doi.org/10.1016/j.coastaleng.2011.08.002.

Rezaei, F., Contestabile, P., Vicinanza, D., Azzellino, A., 2023. Towards understanding environmental and cumulative impacts of floating wind farms: lessons learned from

the fixed-bottom offshore wind farms. Ocean & Coastal Manage. 243. https://doi.org/10.1016/j.ocecoaman.2023.106772.

Tilstone, G.H., Pardo, S., Dall'Olmo, G., Brewin, R.J.W., Nencioli, F., Dessailly, D., et al., 2021. Performance of ocean colour chlorophyll a algorithms for sentinel-3 OLCI, MODIS-aqua and suomi-VIIRS in open-ocean waters of the Atlantic. Remote Sens. Environ. 260, 112444. https://doi.org/10.1016/j.rse.2021.112444.

Venegas, R.M., Acevedo, J., Treml, E.A., 2023. Three decades of ocean warming impacts on marine ecosystems: a review and perspective. Deep Sea Res. Part II 212. https://doi.org/10.1016/j.dsr2.2023.105318.

Wang, L., Wang, B., Cen, W., Xu, R., Huang, Y., Zhang, X., et al., 2024. Ecological impacts of the expansion of offshore wind farms on trophic level species of marine food chain. J. Environ. Sci. 139, 226–244. https://doi.org/10.1016/j.jes.2023.05.002.

Wang, T., Ru, X., Deng, B., Zhang, C., Wang, X., Yang, B., Zhang, L., 2023a. Evidence that offshore wind farms might affect marine sediment quality and microbial communities. Sci. Total Environ. 856. https://doi.org/10.1016/j.scitotenv.2022.158782.

Wang, X., Cai, C., Cai, S.-G., Wang, T., Wang, Z., Song, J., et al., 2023b. A review of aerodynamic and wake characteristics of floating offshore wind turbines. Renew. Sustain. Energy Rev. 175, 113144. https://doi.org/10.1016/j.rser.2022.113144.

Xiong, J., Yin, J., Guo, S., He, S., Chen, J., Abhishek, 2022. Annual runoff coefficient variation in a changing environment: a global perspective. Environ. Res. Lett. 17 (6). https://doi.org/10.1088/1748-9326/ac62ad.

Zeng, X., Shao, Y., Feng, X., Xu, K., Jin, R., Li, H., 2024. Nonlinear hydrodynamics of floating offshore wind turbines: a review. Renew. Sustain. Energy Rev. 191, 114092. https://doi.org/10.1016/j.rser.2023.114092.

Zhang, X., Shi, H., Zhan, C., Zhu, J., Wang, Q., Li, G., 2023. Numerical simulation calculation of thermal discharge water diffusion in coastal nuclear power plants. Atmos. 14 (9). https://doi.org/10.3390/atmos14091371.

Zhao, W., Abhishek, Kinouchi, T., Ang, R., Zhuang, Q., 2022. A framework for quantifying climate-informed heavy rainfall change: implications for adaptation strategies. Sci. Total Environ. 835, 155553. https://doi.org/10.1016/j.scitotenv.2022.155553.

Zheng, Y., Wang, X., Li, S., Dong, G., Wang, Q., Chen, Y., Xue, S., 2024. Numerical simulation model of water quality evolution in urban rivers considering adsorption–desorption process of nitrogen and phosphorus in sediments. J. Hydrol. 636. https://doi.org/10.1016/j.jhydrol.2024.131104.